CPPM - 96-01

C P P M

Centre de Physique
des Particules
de Marseille

CNRS - IN2P3 - Université Aix-Marseille II

LAr electromagnetic energy scale studies using NC DIS (1+1) jet and QED Compton events for the e+p 1994 H1 data

Kermiche S., Marks J.

163, Avenue de Luminy - Case 907
13288 MARSEILLE CEDEX 9 - FRANCE

H1-12/95-466

LAr electromagnetic energy scale studies using NC DIS (1+1) jet and QED Compton events for the e^+p 1994 H1 data

S. Kermiche and J. Marks
Centre de physique des particules de Marseille (CPPM), IN2P3-CNRS
et Université d'Aix-Marseille II, Marseille F-13288, France.

December 7, 1995

Abstract

Two kinds of events in ep collisions, the NC DIS (1+1) jet and the QED Compton events, are used to study the electromagnetic energy scale of the Liquid Argon (LAr) calorimeter of the H1 experiment at HERA. The event samples cover a positron energy range of 2 GeV to 50 GeV. The calibration factor averaged over the CB and BBE part of the LAr calorimeter is measured to be 1.035 ± 0.005 combining the results of both samples. The dependence of the calibration factors on the energy, on the jet angle and on the wheels of the calorimeter are given. A detailed comparison of the measurements and Monte Carlo simulations shows an agreement better than 1 %. The influence of an increased dead material correction is discussed. Finally, an approach to calibrate the central tracking detector is presented. The calibration factor increases linearly with the true transverse momentum ($p_t^{trk}/p_t^{da} = (0.0091 \pm 0.001)p_t^{da} + (0.99 \pm 0.01)$).

Contents

1 Introduction **3**

2 The data samples **3**

2.1 The NC DIS (1+1) jet sample 4

2.2 The QED Compton sample 7

3 The calibration methods **8**

3.1 The double angle method in DIS 11

3.2 The QED Compton method 14

4 The calibration of the LAr calorimeter **14**

4.1 The calibration factors obtained with the NC DIS (1+1) jet sample 14

4.1.1 The dependence of the calibration factor on the energy and the pseudo rapidity 14

4.1.2 The dependence of the calibration factors on the calorimeter wheels . . . 17

4.1.3 The systematic errors 18

4.2 The calibration factors obtained with the QED Compton sample 19

4.2.1 The dependence of κ_G on the energy 19

4.2.2 The dependence of κ_G on the LAr wheels 20

4.2.3 The systematic effects 20

5 The calibration factors - combined results **23**

5.1 The combined results of the QED Compton and DIS NC (1+1) jet sample 23

5.2 The effect of an increased dead material correction 26

6 The calibration of the central tracking system **28**

7 Conclusion **30**

1 Introduction

The energy scale of the calorimeters has an important impact on the analysis of the physics processes studied with the H1 experiment. Two well characterized processes in *ep* collisions, the neutral current (NC) deep inelastic scattering (DIS) (1+1) jet process and the QED Compton process, are used to fix the electromagnetic energy scale of the LAr calorimeter and the central tracking system, taking advantage of their overconstrained final state kinematics. Both combined cover a complementary positron energy range from 2 GeV to 50 GeV. Following this introduction the event samples and their selection are described in the second section. The method of double angle and Compton constraints are discussed in the third section. In the fourth section the results are presented, such as the absolute values of the calibration constants, their various dependencies, like the dependency on the LAr wheels and octants, on the positron energy and on the jet angle. A detailed comparison to Monte Carlo (MC) simulations is also presented in this section. The combined results of the calibration factors for both methods and the effect of an increased dead material correction on these factors are discussed in the fifth section. In the last section and before the conclusion, a short discussion about the calibration of the central tracking system is presented.

2 The data samples

Two different processes, the NC DIS (1+1) jet (1) and the QED Compton (2) process, corresponding to the reactions

$$e + p \rightarrow e + jet_1 + jet_2 \tag{1}$$

$$e + p \rightarrow e + \gamma + p(X) \tag{2}$$

are considered for the calibration of the electromagnetic energy scale.

The naive quark parton model (QPM), where the incident lepton scatters off a quark inside the proton, describes the NC DIS quite well. This should be particularly true in the most simple case of the NC DIS, such as the (1+1) jet process shown in figure 1-a, where the jet of the scattered quark (current jet) and the jet of the proton remnant form the (1+1) jet system. The current jet, the scattered lepton and partly the proton remnant jet are measured in the detector. Two observables are sufficient to describe the kinematics of the process in case of the QPM (assuming the energies of the incident lepton and proton are determined). On the other hand four observables are available, the angle of the scattered lepton θ_e, the angle of the scattered quark γ_q, the energy of the scattered lepton E_e and the energy of the hadronic system E_{had}. Combinations of two of these can be used to determine the kinematics and/or predict the others. Which means, e.g. the energy of the scattered lepton E_e can be determined by an angular measurement, θ_e and γ_q. The requirement to calibrate the LAr calorimeter (θ_e being smaller than about 155 degrees) imposes the usage of a NC sample with Q^2 larger than about 80 GeV^2.

In case of the QED Compton process (figure 1-b) the incident proton radiates a quasi-real photon which does a Compton scattering with the incident positron. The final proton (or hadron)[1] goes in the forward direction, almost without deviation, and escapes in the majority

[1]The elastic channel is dominant, however an inelastic contribution at low Q^2 is expected [3].

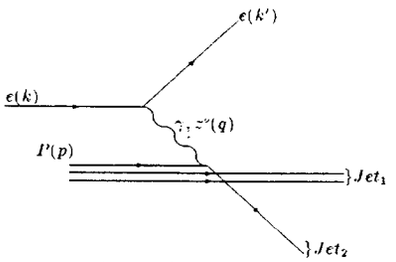

(a) DIS (1+1) jet process

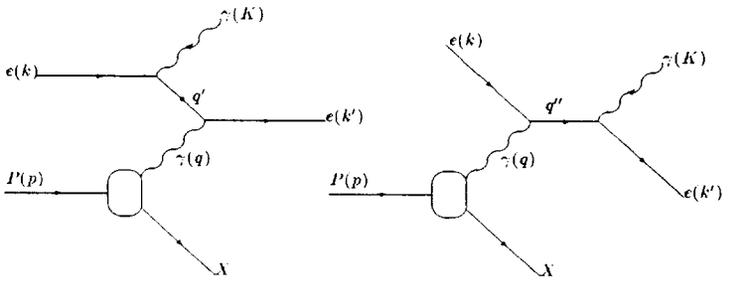

(b) QED Compton process

Figure 1: The processes considered for the calibration of the electromagnetic scale of the LAr calorimeter, a) NC DIS (1+1) jet process, b) QED Compton process.

of the cases the detection at finite angles. This is due to the fact that the quasi-real photon emitted by the incident proton has a very small Q^2 and the intermediate positron is off-shell and has a finite value (not small) [2] of $q'^2(q''^2)$. One observes two electromagnetic particles in the final state, the positron and the photon. This final system is characterized by a very small transverse momentum, and 3 kinematical constraints :

- The final positron and photon are almost coplanar ($\Delta\varphi \simeq \pi$).
- The energies of the final positron E_e and photon E_γ are predictive using only their emission angles (θ_e and θ_γ).

For more details on the Compton process, its characteristics and how the constraints were derived see [1, 2, 3].

In the following the selection of the NC DIS high Q^2 (1+1) jet and the QED Compton sample is described.

2.1 The NC DIS (1+1) jet sample

The NC DIS high Q^2 (1+1) jet event sample was selected from the DST 5/6 positron runs of the data taking period 1994. Only medium and good runs were considered except the shifted vertex runs. In addition the detector status was checked and the LAr big tower timing features were used to remove out of time background [4].

Two sets of NC DIS Monte Carlo data samples, generated with django 2.1 and django 6, were compared (see table 1) to the data.

[2] The expressions "small" and "finite" are with respect to the value of invariant mass $W_{e\gamma}$ produced at the $e\gamma$ vertex.

SET 1	SET 2
DJANGO 2.1 NC DIS	DJANGO 6 NC DIS
820 GeV p , 27.5 GeV e^-	820 GeV p , 27.6 GeV e^+
QCD dipole parton shower	QCD dipole parton shower
$Q^2 > 60$ GeV^2 , $\theta_e < 155^o$	$Q^2 > 60$ GeV^2 , $\theta_e < 155^o$
MRS H	GRV HO
H1SIM 3.06/19	H1SIM 3.06/19
H1DIGIREC 6.00/19	H1DIGIREC 6.00/19

Table 1: The parameter summary of the generated NC Monte Carlo event samples.

Both data and Monte Carlo events were treated the same way: out of the class 9 event sample, events with identified positrons in the LAr calorimeter are selected, which leads to a high Q^2 NC sample. The positron identification is based on cuts on energy density like quantities. The cut parameters are angle and energy dependent and isolation criteria have to be fulfilled. The positron candidate has to have a corresponding track measurement. The efficiency of positron finding in case of the Monte Carlo set 1 was found to be 98 %[3]. Events with positrons hitting the regions of the calorimeter between the wheels and the octants in φ and z, the so called φ and z cracks, are excluded, which is in φ: $\delta\varphi = \pm$ 4 degrees, and in z: $\delta z_{BBE-CB1}$ = [-152.5 cm,-138.5 cm] , $\delta z_{CB1-CB2}$ = [-64.5 cm,-54.5 cm] and $\delta z_{CB2-CB3}$ = [19.0 cm,29.0 cm], because of the energy mis'measurement and the loss in efficiency of the positron finding. For all events a vertex is required. In order to create the (1+1) jet sample the JADE jet finding algorithm is applied using $y_{cut} = 0.02$.

The energy and transverse momentum values are calculated including the LAr calorimeter, BEMC and the tail catcher calorimeter. The energy scale used for the objects measured in the calorimeters is, in case of the positrons, the energy scale after dead material corrections (E_1), and in the case of everything else, the final energy after π^0 weighting (E_f). Beside the π^0 weighting no attempt has been made to treat electromagnetic objects differently, e.g. radiative photons. Every hadronic object[4] in the BEMC and the BBE is scaled by a factor 1.6 and 1.25, respectively, in order to compensate for energy leakage, energy deposition in dead material and the e/π.

The data of the tracking detectors are used for the angular measurements of the positron. The impact position on the calorimeter front face is obtained by an extrapolation using the tracking information.

In addition the following restrictions to the event topology are made:

- the z coordinate of the impact position on the calorimeter front face z_e^{imp} is greater than -190 cm $\Rightarrow$ to exclude the region of overlap between BBE and BEMC
- the current jet angle θ_{jet} is greater than 10^o $\Rightarrow$ to avoid energy leakage in the beam hole area
- the measured energy in the BEMC (E_{BEMC}) is smaller than 0.1 GeV $\Rightarrow$ to exclude events with hadronic energy leakage in the backward area
- the quantity $\sum_h (E^h - p_z^h)$ is greater than 44 GeV $\Rightarrow$ to exclude radiative DIS and photoproduction events

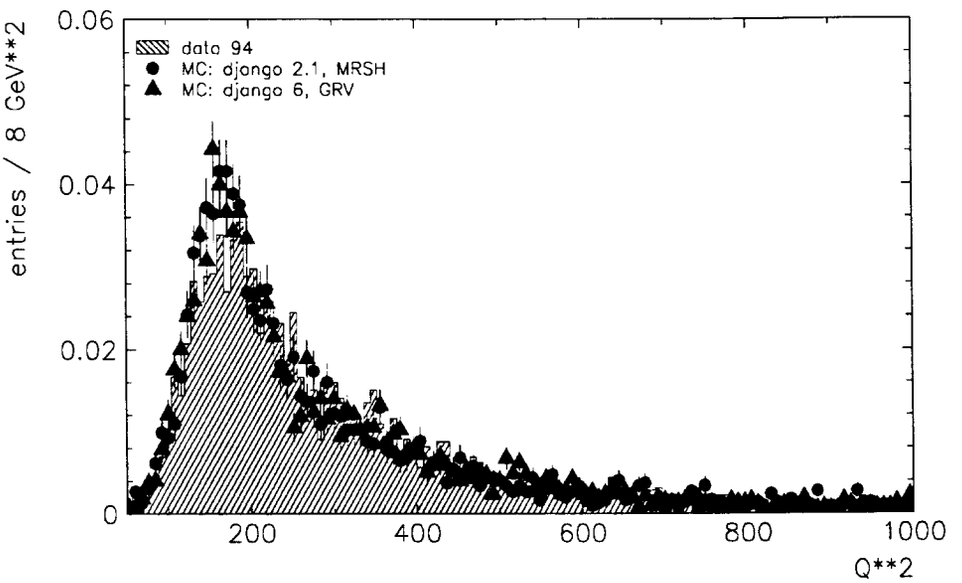

(a) Q^2 distributions.

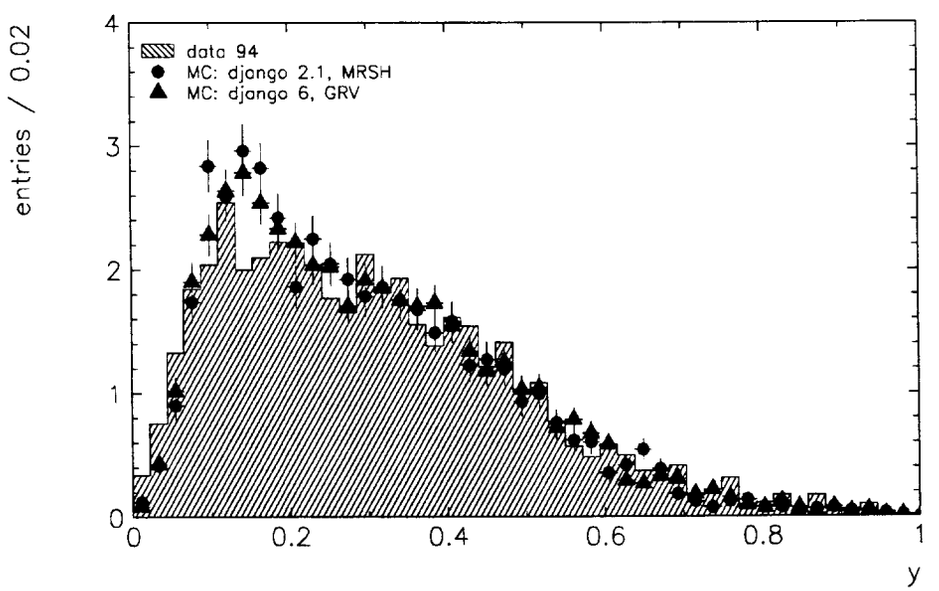

(b) y distributions.

Figure 2: The Q^2 and y distributions of data and both Monte Carlo sets for NC DIS (1+1) jet events after selection.

sample	N^o events
data	3140
MC - set 1	2931
MC - set 2	7311

Table 2: The number of NC DIS (1+1) jet events after the selection.

The number of events after selection for the different samples is shown in table 2.

The selection and the statistical limits of the DIS process restrict the area of the detector in which a calibration with the double angle method can be obtained to the CB and BBE area of the LAr calorimeter.

The measured Q^2 and y distributions following the selection agree reasonably well with both Monte Carlo sets as shown in figure 2.

2.2 The QED Compton sample

The QED Compton event sample was selected from positron runs of the 1994 data taking period using the COMPTON minipot selection (class 12 bit 5, old classification, see appendix): MPOT5.COMPTON.A00-B06.

The initial Monte Carlo sample contains 10000 events; it was generated by COMPTON 2.00/00 [5, 6, 7], simulated with the H1 standard simulation program H1SIM 3.06/19 (fast option) and reconstructed by the reconstruction program H1REC 6.00/19.

After applying the new event classification scheme, described in the appendix, 14767 candidates out of the whole positron sample were selected. Keeping only events with one particle hit in the BEMC and the other one in the LAr calorimeter reduces the sample to 7057 events. In the following additional selection steps are listed:

1) The shifted vertex runs are not considered in this study. The events having one of the two clusters in an area where the cluster position is not well defined, as in the triangular area of the BEMC, in the BEMC/BBE overlap region and in the z-crack regions of the LAr, are excluded.

2) Since the LAr calorimeter should be calibrated no QED Compton constraint is used on the LAr cluster. Only the constraint on the BEMC cluster is used in the cut defined by :

$$\chi^2_{bemc} = \left(\frac{E_{cl}^{bemc}(\theta) - E_{cl}^{bemc}}{0.3\sqrt{E_{cl}^{bemc}(\theta)}} \right)^2 \leq 5 \qquad (3)$$

where $E_{cl}^{bemc}(\theta)$ is the predicted energy of the BEMC cluster derived from the kinematical constraints (see section 3). The figure 3-a shows the distribution of χ^2_{bemc} after cut (1).

[3] More details will be given together with the program package to be released later.

[4] Which means technically every cluster which is not a cluster that belongs to the identified positron.

3) Only electromagnetic LAr clusters should be used. The following estimator is defined:

$$EMES = \sum_{i=1}^{ncel} \frac{type^i_{cel} \times E^i_{cel}}{\sum_{i=1}^{ncel} E^i_{cel}} \tag{4}$$

which is based on the cell information of the DCEL bank, where each of the *ncel* cells of the LAr cluster is classified in one of the four classes : the undefined cells (type=0), the electromagnetic cells (type=1), the hadronic cells (type=2) and the garbage cells (type=3). For electromagnetic clusters $EMES$ is about one, which results then in a cut: $EMES \leq 1.5$. The figure 3-b shows the distribution of this variable after cut (1).

4) The LAr cluster must be linked to one, and only one, track. This isolation criterion assures that one uses only the positrons to calibrate the calorimeter, because preshowering between photons and positrons is different and gives different calibration factors for photons and positrons at the same energies. The isolation estimator is defined as:

$$\Delta = \sqrt{(\theta_{cl} - \theta_{track})^2 + (\varphi_{cl} - \varphi_{track})^2} \tag{5}$$

This study requires an isolated track pointing to the positron in the LAr: $\Delta_{track} \leq 5^o$, for one track, and if there is more than one track: $\Delta_{other-tracks} > 45^o$. The events without track are excluded.

5) Finally, in order to have a clean sample, a scanning event by event is performed. This removes another 10 % of the events.

The final sample, used in this study, contains in case of data 290 events and in case of Monte Carlo 1366 events. A schematic distribution of the positions of the two balanced clusters (between BEMC and LAr) of the selected events is shown in figure 3-c for the data. In about 80 % of the cases the positron is the particle emitted in the LAr acceptance and the photon the one in the BEMC acceptance. The Compton scattering process prefers the back-scattering in the center of mass of the $e\gamma^* \rightarrow e\gamma$ reaction. In the laboratory frame, due to the large Lorentz boost[5], the final photon will have the tendency to go very backward at large θ and the final positron will be also emitted backward, but at lower angles than the photon.

The figure 4 shows a good agreement between data and Monte Carlo for the three distributions, the energy of the positron in LAr E_e, its polar (θ_e) and azimuthal (φ_e) angles.

3 The calibration methods

For both the NC DIS and the QED Compton process the energy-momentum conservation leads to the similar relation, giving the energy of the final positron as function of the scattering angles θ_e and γ_q for the NC DIS or θ_e and θ_γ for the QED Compton:

$$E_e(\theta_e, \theta) = \frac{2E_o \sin\theta}{\sin\theta_e + \sin\theta - \sin(\theta_e + \theta)} \tag{6}$$

where θ is the quark angle γ_q in case of the NC DIS process and the final photon angle θ_γ in case of the QED Compton process; E_o is the incident lepton energy. In the following, the predicted

[5]Because the energy of the quasi-real photon is dominated by the small energies, since its distribution varies as $dE_{\gamma^*}/E^2_{\gamma^*}$, where $E^{min}_{\gamma^*} \sim 32$ MeV.

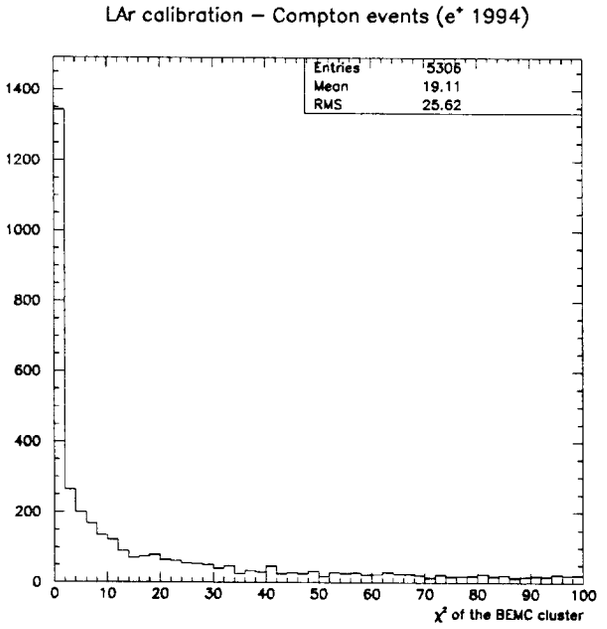

(a) The χ^2_{BEMC} distribution used to constraint the BEMC cluster.

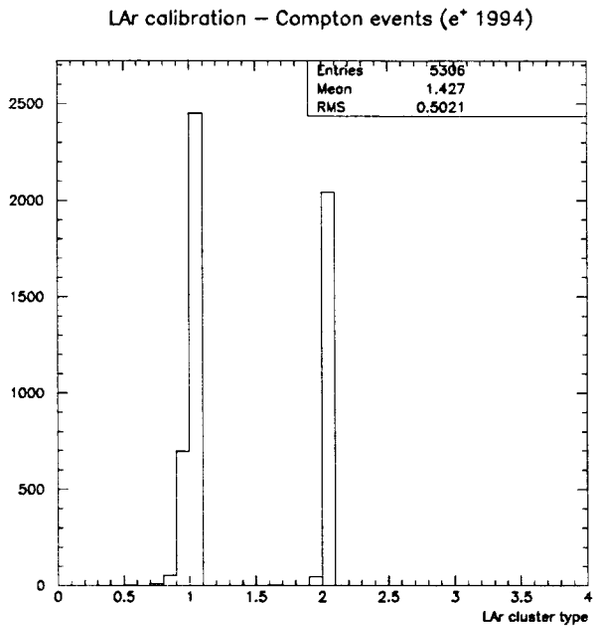

(b) The estimator $EMES$ separating electromagnetic and hadronic clusters.

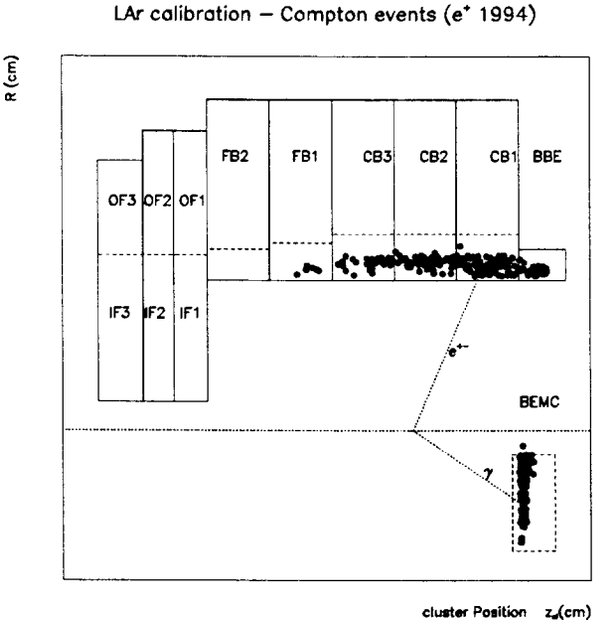

(c) The balanced clusters between LAr and BEMC for the final data sample.

Figure 3: The Compton estimators distributions (a) and (b) and a schematic view of the cluster positions for the final data sample (c).

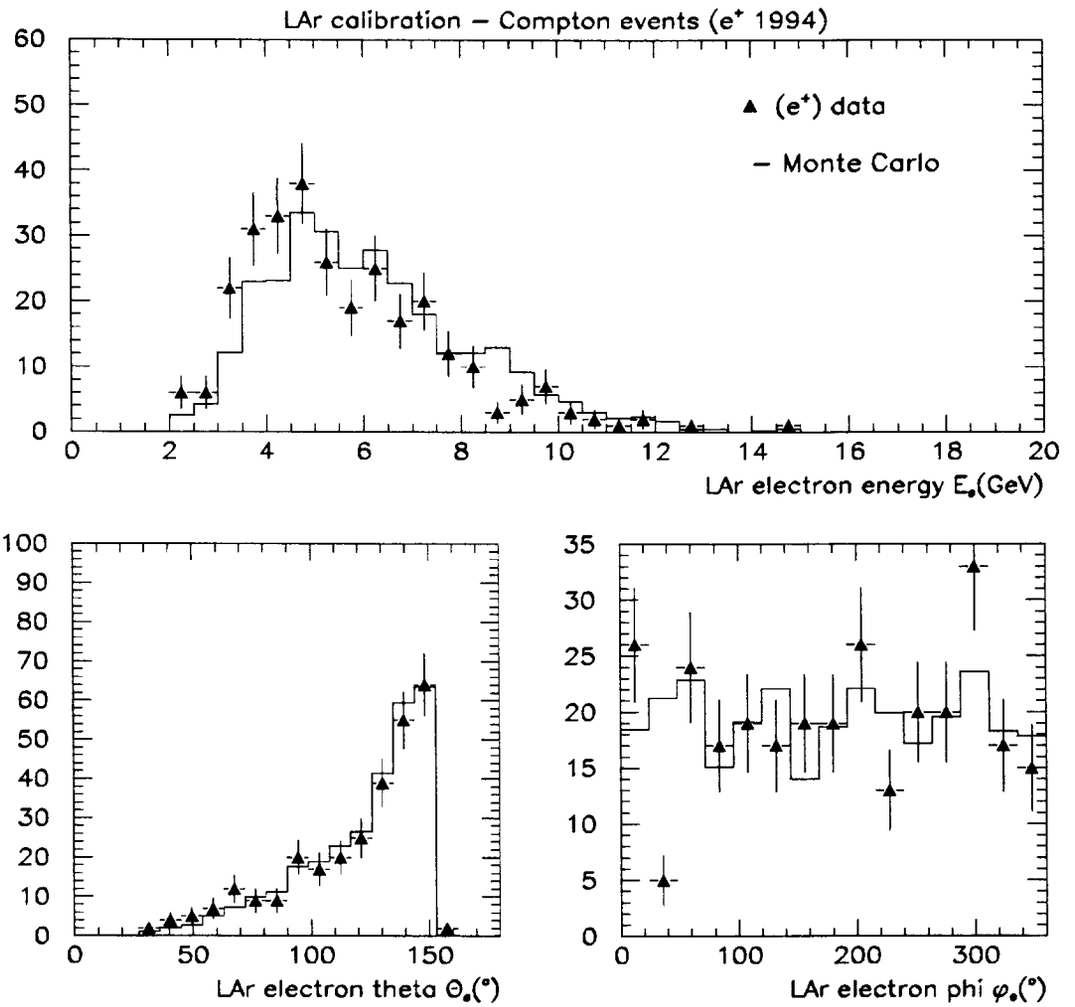

Figure 4: The data and Monte Carlo comparisons for the final sample: the energy E_e, the angles θ_e and φ_e of the positron in the LAr.

DIS positron energy $E_e(\theta_e, \gamma_q)$ will be denoted E_e^{da} and the predicted Compton positron energy $E_e(\theta_e, \theta_\gamma)$ will be denoted $E_e(\theta)$. If not specified E_e^{da} means the predicted energy of both methods.

The quantity

$$\zeta = \frac{(\frac{E_e^{da}}{E_e})_{data}}{(\frac{E_e^{da}}{E_e})_{MC}} \tag{7}$$

will be taken to define the relative deviation of data with respect to Monte Carlo for both the processes.

3.1 The double angle method in DIS

While the angle of the scattered positron is measured quite precisely by the tracking chambers, the angle of the struck quark is not observed directly. But rather reconstructed from the final state hadrons after fragmentation of the quarks and gluons [8],[9].

$$\tan\frac{\gamma_q}{2} = \frac{\sum_h (E^h - p_z^h)}{\sqrt{(\sum_h p_x^h)^2 + (\sum_h p_y^h)^2}} \tag{8}$$

In this representation global calibration errors cancel and only local miscalibration enters, and can be considered as second order effect. Hence, the energy of the scattered positron can be determined in a way which is in first order independent of any energy scale, which means that the DIS process can be used to determine an absolute energy scale of the positron. A comparison with the energy measurement of the scattered positron in the calorimeters allows a determination of the calibration factors.

In order to illustrate the method, figure 5-a shows the ratio of the predicted energy by the double angle method to the true positron energy at the generator level E_e^{da}/E_e^{gen} in case of a sample of DIS NC Monte Carlo events. As expected, the peak of the distribution is found to be 1.0.

The calibration factors quoted in the following are defined as the ratio of the predicted positron energy by the double angle method E_e^{da} to the measured positron energy in the LAr calorimeter E_e . Clearly, these factors depend on the evaluation method of the distributions. In most cases the mean value obtained from Gaussian fits to the increasing part of the distributions[6] will be used.

In order to understand the meaning of the calibration factors determined by the double angle DIS method, it should be noted that the definition of the physics objects and their properties, like e.g. positrons, depends on the particular analysis. In this sense, the calibration factors are not necessarily absolute values. They are valid for a specific type of analysis. But, more important, the calibration factors need to be reproduced by Monte Carlo simulations. It has to be seen to which extend the data can be described by the simulation.

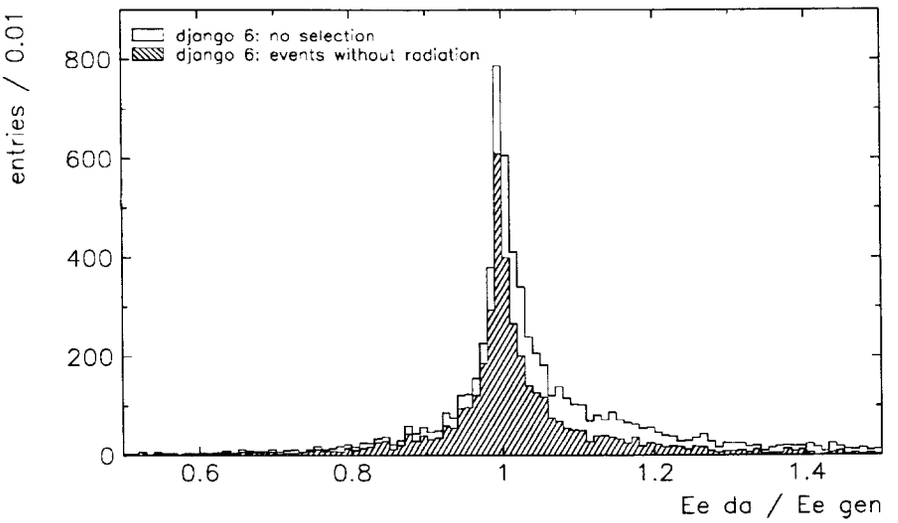

(a) Distributions of E_e^{da}/E_e^{gen} for Monte Carlo data (django 6) without selection. The hatched distribution shows E_e^{da}/E_e^{gen} for events without radiative process.

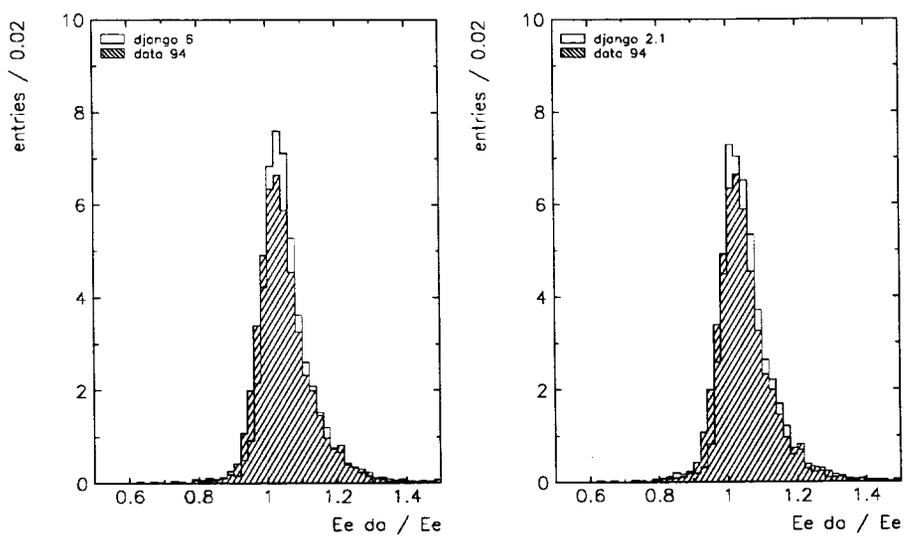

(b) Distributions of E_e^{da}/E_e for data and both Monte Carlo datasets (NC DIS (1+1) jet events) after selection.

Figure 5: The ratio of the double angle energy prediction to the positron energy (E_e^{da}/E_e), (a) at the generator level, (b) after reconstruction and selection, for the data and the two Monte Carlo samples.

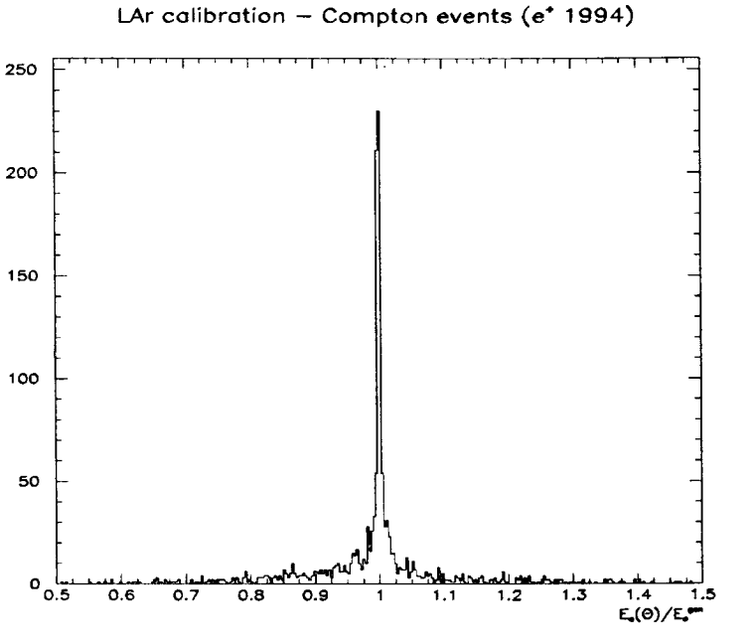

(a) The ratio $E_e(\theta)/E_e^{gen}$ for the Compton sample.

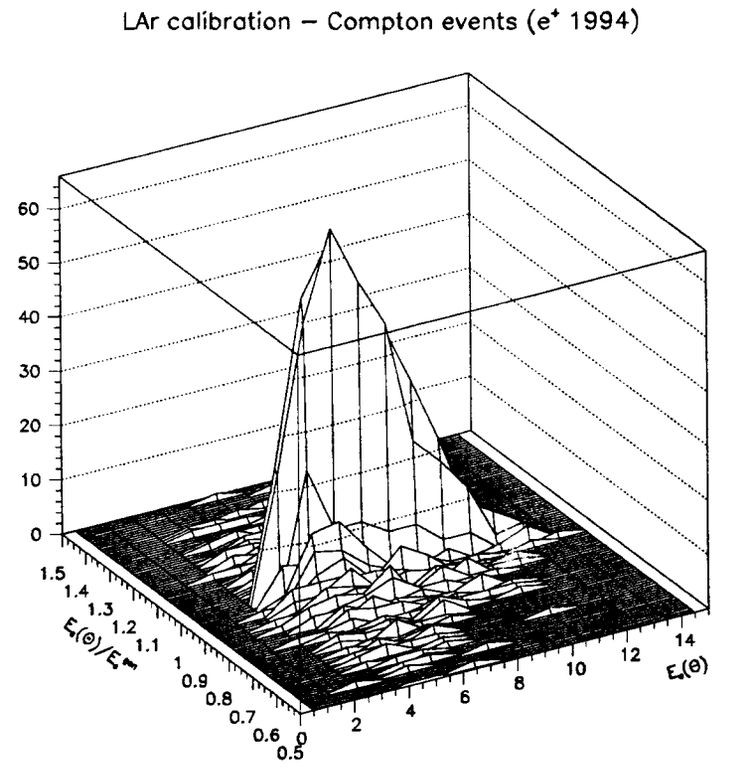

(b) The ratio $E_e(\theta)/E_e^{gen}$ as function of the predicted energy.

Figure 6: The ratio of the predicted Compton energy to the energy at the generator level ($E_e(\theta)/E_e^{gen}$) (a) and its energy dependence (b).

3.2 The QED Compton method

The idea of using the QED Compton events for calorimeter calibration has been proposed previously [1, 2]. For the H1 experiment it has been applied the first time in 1992 to calibrate the BEMC [10]. For the 1993 data the calibration of the same calorimeter has been performed with more statistics [3, 11, 12].

The calibration factor, as for the double angle method, is defined as the "optimum" of the ratio between the predicted energy and the measured one: $E_e(\theta)/E_e^{LAr}$, where E_e^{LAr} is the LAr cluster energy, obtained from DCEL bank using the E_1 scale. The calibration factor is the mean value of a Gaussian fit to the distribution $E_e(\theta)/E_e^{LAr}$ and is denoted as κ_G.

The figure 6-a shows the ratio of the expected Compton energies obtained from equation 6 to the generated positron energies. The peak position, which is found to be one, confirms that the method provides proper results. No dependence of the peak on the expected Compton energy is found (figure 6-b).

The QED Compton method has the advantage to use only electromagnetic particles, so it is independent of the hadronic part of the LAr calorimeter.

4 The calibration of the LAr calorimeter

4.1 The calibration factors obtained with the NC DIS (1+1) jet sample

The figure 5-b shows the distributions of the ratio of the predicted energy by the double angle method E_e^{da} to the measured positron energy E_e. The measurement (hatched distribution) is compared to both Monte Carlo datasets. The asymmetry of the distributions (more entries in the upper part) is to a large extend due to radiative events. This is demonstrated in figure 5-a, where the distribution of the ratio of the double angle energy to the positron energy on the generator level E_e^{da}/E_e^{gen} without radiative events is compared to the distribution of all events. The distribution without radiative process appears to be symmetrical.

As calibration factor for the entire LAr calorimeter $E_e^{da}/E_e = 1.028 \pm 0.001$ [7] is obtained from a Gaussian fit to the rising edge of the distribution in figure 5-b. The width of the fit is found to be $\sigma = 0.052$. A Gaussian fit to the decreasing part of the distribution gives $E_e^{da}/E_e = 1.034 \pm 0.002$ with $\sigma = 0.073$.

Comparing the E_e^{da}/E_e distributions of the Monte Carlo simulations to the data the agreement appears to be good. The MC distributions peak at slightly higher values and the deviation of the MC-set 1 from the data is found to be $\zeta = 0.993 \pm 0.001$ and of MC-set 2 $\zeta = 0.992 \pm 0.001$. The width appears to be 20% smaller for both MC datasets.

4.1.1 The dependence of the calibration factor on the energy and the pseudo rapidity

The figure 7-a shows the calibration factor in four bins of the double angle positron energy over an energy range of 10 GeV to 50 GeV. The calibration factor decreases with increasing energy

[6] A typical range is [0.6,1.1].

[7] The error is the statistical one only.

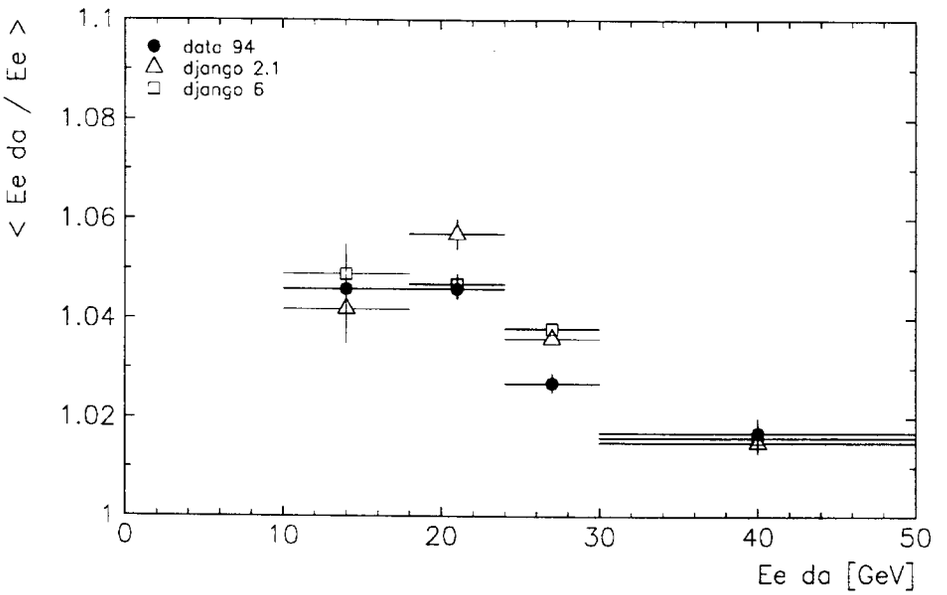

(a) E_e^{da}/E_e in various bins of the double angle positron energy E_e^{da} for both data and Monte Carlo.

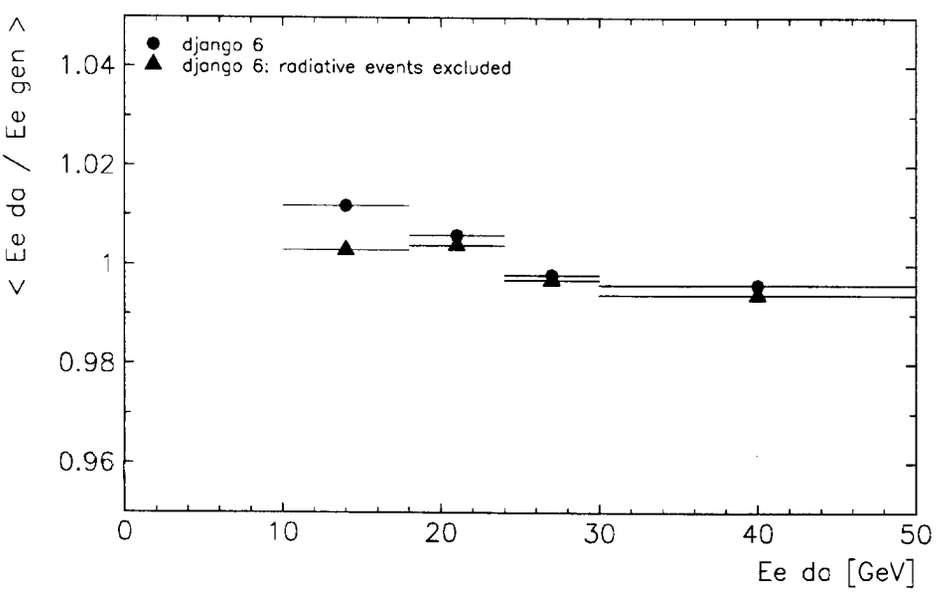

(b) The dependence of E_e^{da}/E_e^{gen} on the double angle positron energy E_e^{da} in case of Monte Carlo (django 6).

Figure 7: The calibration factor E_e^{da}/E_e as function of the positron double angle energy : (a) For data and the two Monte Carlo samples after reconstruction and selection, (b) at the generator level.

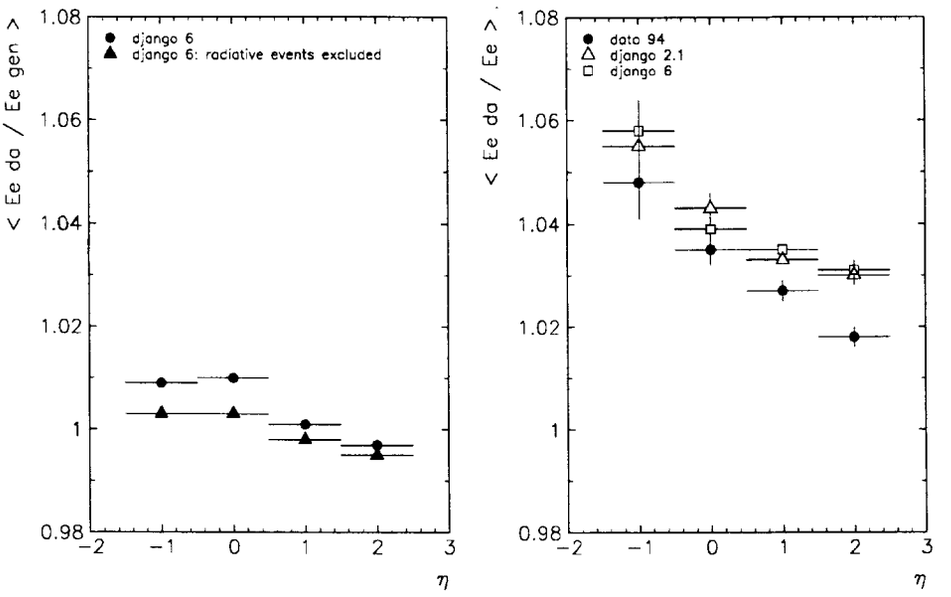

(a) The dependence of E_e^{da}/E_e^{gen} on the pseudo rapidity of the jet η_{jet} in case of Monte Carlo.

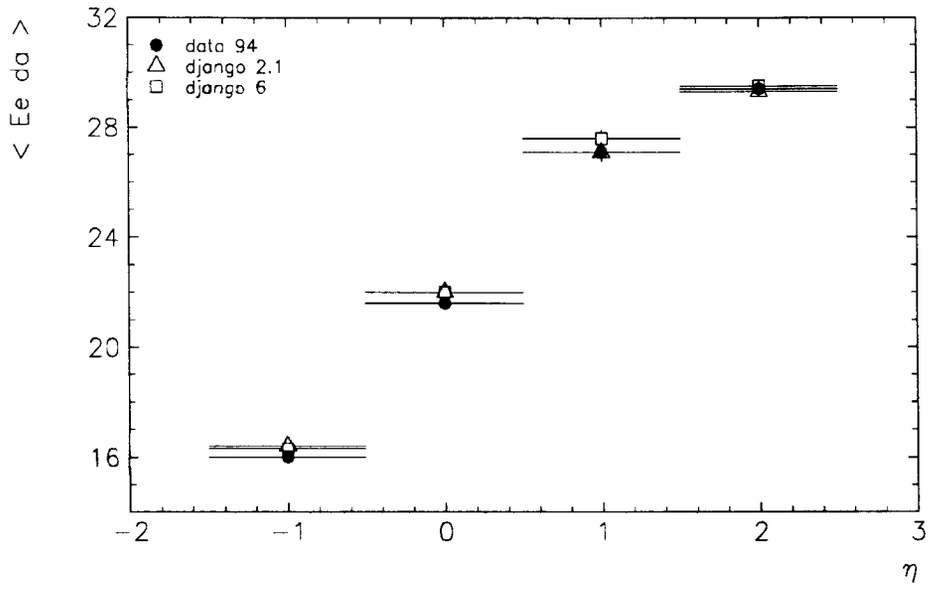

(b) Average double angle energy prediction in various bins of the pseudo rapidity η_{jet} for both data and Monte Carlo.

Figure 8: The dependence of the calibration factor on the energy of the positron and on the jet angle. Monte Carlo and data comparison.

by 0.03. Comparing data and Monte Carlo the energy dependence is described reasonably well for both Monte Carlo datasets. However, deviations on the 1 % level are observed in the energy range of 20 GeV to 30 GeV for both Monte Carlo datasets.

In order to check the energy dependence of the double angle method the quantity E_e^{da}/E_e^{gen} is considered in the same four double angle energy bins. In figure 7-b $< E_e^{da}/E_e^{gen} >$ is given as peak position of the distributions for all selected Monte Carlo events and events without radiative process. The energy dependence observed shows the limitations of the DIS double angle calibration method. The double angle method seems to overestimate the energy in the low energy regime and to underestimate at high energies. The maximum difference is 0.016, in case of all selected events. Considering the events without radiative process the maximum deviation is reduced to 0.011.

The dependence of E_e^{da}/E_e on the pseudo rapidity of the jet η_{jet} is shown in the right part of figure 8-a. Sweeping the jet angle over the full range of the LAr calorimeter changes the calibration factor by 0.03. In general, the Monte Carlo simulations describe the dependence, but deviations on the 1 % level appear in case the jet points forward. The average double angle positron energy in four η bins is shown in figure 8-b. The average positron energy decreases with increasing jet angle.

Since the η dependence could be caused by the hadronic system, $< E_e^{da}/E_e^{gen} >$ as function of η_{jet} is considered for the django 6 sample (left part of figure 8-a). The maximum difference observed in case of all selected events is 0.011. Using only the events without radiative process, the maximum difference decreases to 0.008. As discussed already in the context of the energy dependence, these numbers are a measure for the limit of the double angle method.

4.1.2 The dependence of the calibration factors on the calorimeter wheels

The table 3 summarizes the calibration factors in various parts of the LAr calorimeter. The variation from wheel to wheel stays well within 1.5 %.

	data 94		MC-set 1		MC-set 2	
	$\frac{E_e^{da}}{E_e}$	$\sigma(\frac{E_e^{da}}{E_e})$	$\frac{E_e^{da}}{E_e}$	$\sigma(\frac{E_e^{da}}{E_e})$	$\frac{E_e^{da}}{E_e}$	$\sigma(\frac{E_e^{da}}{E_e})$
BBE	1.021 ± 0.003	0.054	1.052 ± 0.003	0.043	1.055 ± 0.003	0.046
CB1	1.035 ± 0.002	0.045	1.026 ± 0.002	0.038	1.027 ± 0.001	0.041
CB2	1.025 ± 0.003	0.048	1.022 ± 0.002	0.038	1.022 ± 0.002	0.037
CB3	1.036 ± 0.010	0.055	1.040 ± 0.013	0.056	1.026 ± 0.005	0.029
all	1.028 ± 0.001	0.052	1.035 ± 0.001	0.043	1.036 ± 0.001	0.044

Table 3: The calibration factors in various parts of the LAr calorimeter.

In the BBE area, the Monte Carlo response is found to be 3 % too small (see table 4) compared to data, while in the CB area, the agreement of data and Monte Carlo is better than 1 %.

In the BBE and CB1 of the LAr calorimeter the statistics are sufficient to look for stack to stack variations of the response to positrons. The results are summarized in table 5. In case of data, the maximum variation in BBE is 4.1 % and in CB1 4.0 %, in case of Monte Carlo, the maximum variations is about a factor three smaller.

Calor. part	ζ MC set 1	ζ MC set 2
BBE	0.972 ± 0.004	0.968 ± 0.004
CB1	1.009 ± 0.003	1.008 ± 0.002
CB2	1.003 ± 0.004	1.002 ± 0.004
CB3	0.996 ± 0.013	1.010 ± 0.011

Table 4: The ratio of data to Monte Carlo in various parts of the LAr calorimeter.

BBE	data 94		MC-set 1		MC-set 2	
Octant	$\frac{E_e^{da}}{E_e}$	$\sigma(\frac{E_e^{da}}{E_e})$	$\frac{E_e^{da}}{E_e}$	$\sigma(\frac{E_e^{da}}{E_e})$	$\frac{E_e^{da}}{E_e}$	$\sigma(\frac{E_e^{da}}{E_e})$
0	1.011 ± 0.005	0.060	1.056 ± 0.006	0.051	1.061 ± 0.006	0.053
1	1.047 ± 0.008	0.068	1.060 ± 0.005	0.046	1.062 ± 0.005	0.053
2	1.021 ± 0.006	0.059	1.060 ± 0.005	0.046	1.062 ± 0.005	0.050
3	1.021 ± 0.006	0.057	1.059 ± 0.005	0.049	1.053 ± 0.004	0.042
4	1.025 ± 0.007	0.069	1.058 ± 0.005	0.050	1.057 ± 0.004	0.048
5	1.033 ± 0.005	0.055	1.054 ± 0.006	0.050	1.055 ± 0.005	0.059
6	1.052 ± 0.020	0.088	1.064 ± 0.007	0.052	1.067 ± 0.006	0.055
7	1.033 ± 0.008	0.063	1.060 ± 0.006	0.051	1.060 ± 0.005	0.046
CB1	data 94		MC-set 1		MC-set 2	
0	1.034 ± 0.004	0.045	1.035 ± 0.004	0.045	1.032 ± 0.003	0.050
1	1.050 ± 0.006	0.051	1.026 ± 0.004	0.046	1.022 ± 0.004	0.047
2	1.048 ± 0.004	0.051	1.036 ± 0.004	0.047	1.031 ± 0.004	0.046
3	1.026 ± 0.004	0.044	1.022 ± 0.004	0.047	1.033 ± 0.004	0.040
4	1.032 ± 0.006	0.063	1.032 ± 0.004	0.047	1.031 ± 0.003	0.043
5	1.061 ± 0.004	0.040	1.027 ± 0.004	0.039	1.032 ± 0.004	0.047
6	1.054 ± 0.008	0.060	1.030 ± 0.006	0.049	1.025 ± 0.005	0.047
7	1.021 ± 0.004	0.048	1.034 ± 0.004	0.044	1.029 ± 0.003	0.041

Table 5: The calibration factors of BBE and CB1 for different octants.

4.1.3 The systematic errors

The errors in the previous figures and on the numbers quoted so far were of statistical nature only.

Systematic effects due to the double angle method can be evaluated by considering the ratio of the predicted double angle positron energy to the positron energy from the generator E_e^{da}/E_e^{gen}. In section 4.1.1 the figure 7-a was discussed, which shows the energy dependence of E_e^{da}/E_e^{gen}. The maximum difference is found to be 0.016 in case of all selected events. This variation is due to the double angle method itself and probably related to the determination of γ_q. The maximum difference decreases to 0.011 in the case when events without radiative process are considered. In principle, a correction for this effect would be necessary or the maximum difference has to be treated as systematic error of the method in case of a consideration of the energy dependence.

Since the events, which include the radiative process, are found to a large extend in the tail area of the distribution E_e^{da}/E_e, the influence of the radiative process on the peak position has to be evaluated (see figure 5). A comparison of the peak position of the distributions E_e^{da}/E_e^{gen} on the generator level, in case of all events and events without radiative process, shows no change of the peak position, which is evaluated by a peak finder to be $(E_e^{da}/E_e^{gen})_{peak} = 0.997$. Applying the selection criteria used in this note, the same value of $(E_e^{da}/E_e^{gen})_{peak}$ is found. In case of the

e^+ energy	κ_G^{data}	κ_G^{MC}	$\kappa_G^{data}/\kappa_G^{MC}$
[2,4.5[	1.036 ± 0.019	1.049 ± 0.009	0.988 ± 0.020
[4.5,7[	1.058 ± 0.012	1.052 ± 0.005	1.006 ± 0.012
[7,16[	1.051 ± 0.015	1.048 ± 0.006	1.003 ± 0.015
All	1.048 ± 0.008	1.051 ± 0.004	0.997 ± 0.009

Table 6: The calibration factors and the ratio of data to Monte Carlo in various energy bins.

average calibration factor of the LAr calorimeter, a correction due to radiative effects does not seem to be necessary and the errors can be absorbed in the error in the determination of the peak value of the asymmetric distributions of E_e^{da}/E_e.

A source of error in terms of an absolute value of the calibration factor, including the contribution of the radiative process and the γ_q determination, is due to the method of evaluating the distribution E_e^{da}/E_e. As shown in figure 5-b this distribution is asymmetrical with a tail due to radiative events and events with energy losses. Obviously, a symmetric Gaussian fit including the tails will cause a big sensitivity of the calibration factor on changes in the tail area. Fitting the peak position from the upper edge of the distribution and from the lower edge leads to a difference in the peak positions of $\delta = 0.006$ (see section 4.1). This value can be interpreted as a systematic error in terms of an absolute value of the calibration factor.

4.2 The calibration factors obtained with the QED Compton sample

The figure 9 shows the distribution of the ratio of the predicted Compton energy to the measured energy for both data (a) and Monte Carlo simulation (b). The curves correspond to Gaussian fits around the peak of the distribution. The results are as follows:

- Data : $\kappa_G = 1.048 \pm 0.008$
- Monte Carlo : $\kappa_G = 1.051 \pm 0.004$
- The ratio : $\zeta = \kappa_G^{data}/\kappa_G^{MC} = 0.997 \pm 0.009$

A good agreement between data and Monte Carlo is observed, but the electromagnetic scale has to be corrected in both cases on the 5 % level.

4.2.1 The dependence of κ_G on the energy

The energy spectrum of the positrons of the QED Compton events is in the range of 2 GeV to 16 GeV with a mean value of about 5 GeV (see figure 4). The figure 10-a and table 6 show the calibration factor (κ_G) in three energy bins ($E_e(\theta)$): [2.,4.5[, [4.5,7.[and [7.,16.[. Within the errors the calibration factor is measured to be independent of the energy. The ratio of the calibration factor of data to Monte Carlo simulation (ζ) is found to be one within the errors (see table 6). Hence, the agreement of data and Monte Carlo is quite good.

LAr wheels	κ_G^{data}	κ_G^{MC}	$\kappa_G^{data}/\kappa_G^{MC}$
BBE	1.071 ± 0.024	1.081 ± 0.009	0.991 ± 0.024
CB1	1.065 ± 0.011	1.053 ± 0.005	1.011 ± 0.011
CB2	1.035 ± 0.015	1.045 ± 0.006	0.990 ± 0.015
CB3	0.997 ± 0.050	0.989 ± 0.017	1.008 ± 0.053
All	1.048 ± 0.008	1.051 ± 0.004	0.997 ± 0.009

Table 7: The calibration factors and data to Monte Carlo ratio by LAr wheels.

4.2.2 The dependence of κ_G on the LAr wheels

One can separate the contribution of the different parts of the LAr calorimeter to the calibration factor. The figure 10-b and table 7 show the dependence of the calibration factor on the LAr wheels. Again, data and Monte Carlo agree well (at the level of the 1%) and, for both, the correction factor is higher for the BBE than the other CB wheels. Table 7 and figure 10-d show the dependence of the data to Monte Carlo ratio (ζ) with the LAr wheels confirming their agreement.

4.2.3 The systematic effects

Since the predicted energy used for the calibration depends only on the beam energy and the final particle angles, a systematic error could come from radiative corrections, which reduce the value of E_o, or from a wrong measurement of the cluster positions. The first source of errors, radiative corrections, could be studied with Monte Carlo events, because in this case one can take into account the radiated photon energy and get the real incident positron energy. Including the radiation, the calibration factors given above change at maximum by 1%. Compared to the statistical errors ($\simeq 2\%$), the error due to theta determination is very small. These mis-'measurments of $E_e(\theta)$ contribute to the tails of the distributions. Studying these tails will give an idea about these systematics.

For cross-checks two other methods can be used to get the LAr calibration factors, which include the tails of the distributions.

The mean value method : This method considers the mean value κ of the ratio $E_e(\theta)/E_e$ as calibration factor.

The distributions in figures 9-a,b show a mean value of 1.048 for the data (a) and 1.092 for Monte Carlo (b). Using the Gaussian fit values as reference the following ratios are obtained :

- Data : $\kappa/\kappa_G = 1.000 \pm 0.013$
- Monte Carlo : $\kappa/\kappa_G = 1.039\% \pm 0.007$

Data and Monte Carlo disagree by $\sim 4\%$ which means that the Monte Carlo is not able to reproduce the tails of distributions.

The figures 11-a,c show the dependence of the ratio κ/κ_G on the energy and on the LAr wheels. If one compares data and Monte Carlo, one sees in the figure 11-a that the first energy

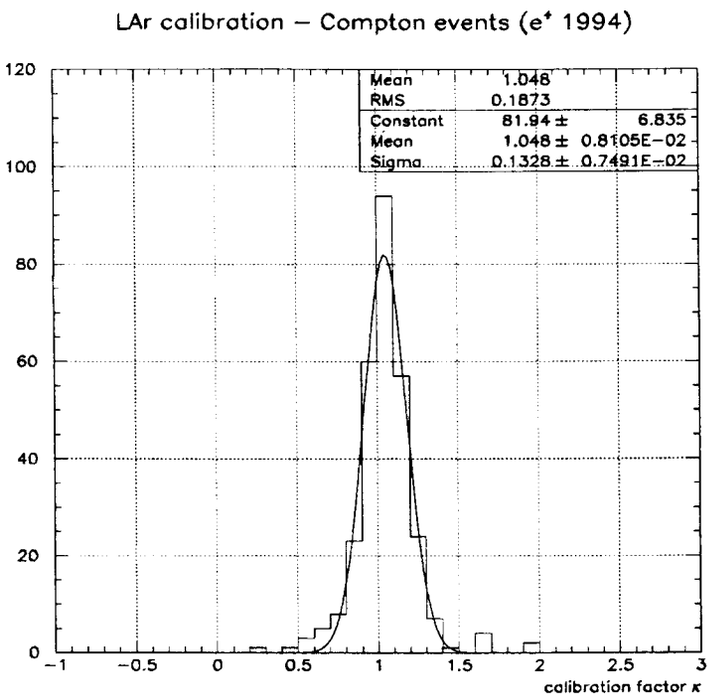

(a) Data.

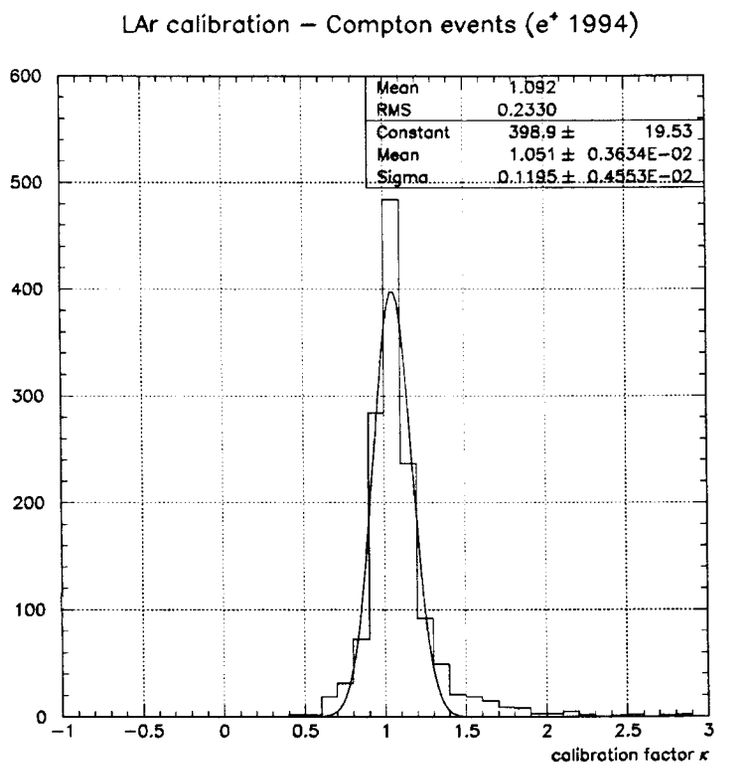

(b) Monte Carlo.

Figure 9: The distributions of calibration factor $(E_e(\theta)/E_e)$ for data and Monte Carlo.

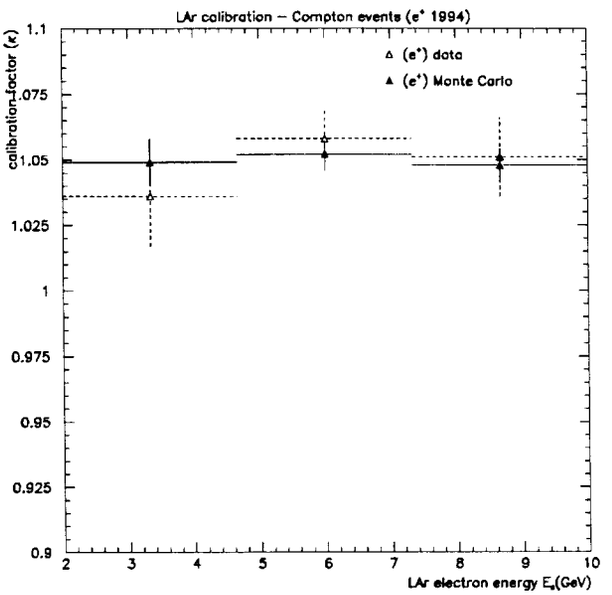

(a) The calibration factor dependence with the energy.

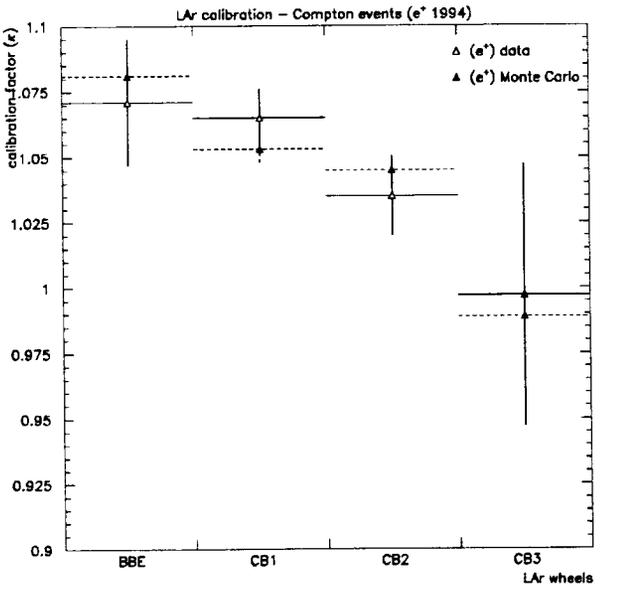

(b) The calibration factor dependence with LAr wheels.

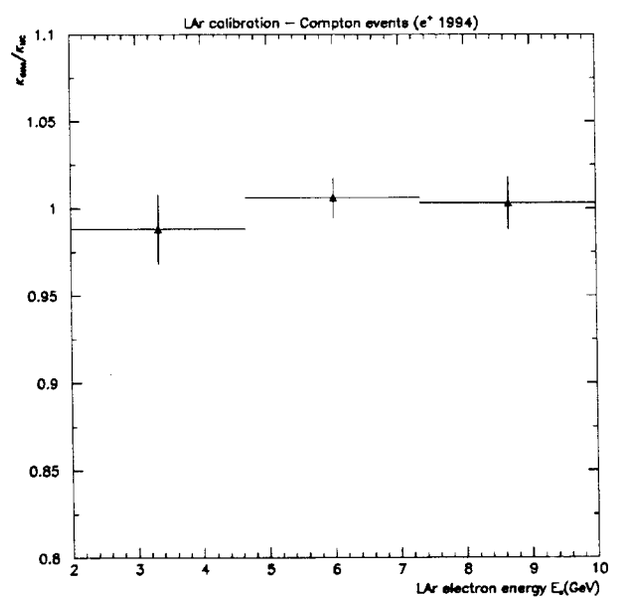

(c) The ratio of the calibration factors $\kappa_{data}/\kappa_{Monte\ Carlo}$ in various energy bins.

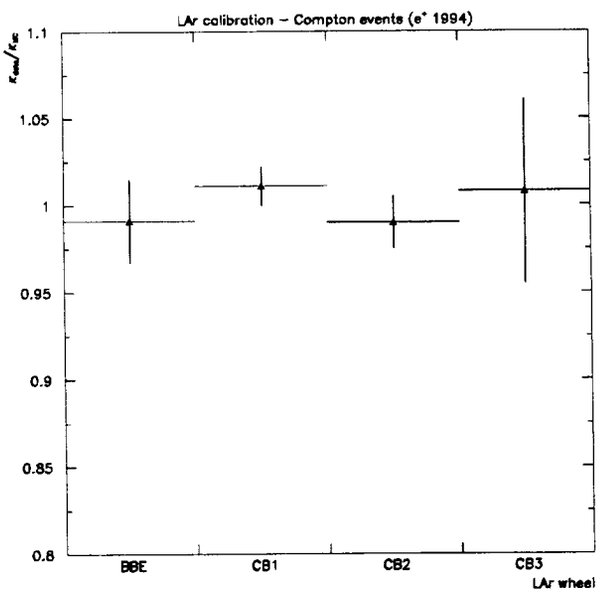

(d) The ratio of the calibration factors $\kappa_{data}/\kappa_{Monte\ Carlo}$ by LAr wheels.

Figure 10: The dependence of the calibration factor and the data to Monte Carlo ratio, with the energy and the LAr wheels.

bin shows a difference of $\simeq 5\%$. This means that the Monte Carlo is not able to describe the tails coming from low energy positrons. This difference is smaller for the two other energy bins, 3% and 2% respectively. In all cases the Monte Carlo ratios stay below the data ones and the behaviour of the distributions is the same for both.

The wheel dependence of the ratio (κ/κ_G) (figure 11-c) shows a data-Monte Carlo discrepancy of $\simeq 6\%$ in the CB area. This matches the previous result found in the lowest energy bin. Due to p_t balance reasons, the lower is the θ of the cluster the lower is its energy, so the CB part contains the lower energies of the spectrum.

In the following as the systematic error of the calibration factor (QED Compton) the difference between the mean value method and the Gaussian fit method ($|\kappa - \kappa_G|$) is used.

The χ^2 method : Considering that the distributions are Gaussian, one can get the calibration factor (κ_2) by minimizing the value of :

$$\chi^2 = \sum_{i=1}^{Nevt} \left(\frac{E^i_{cl1}(\theta) - \kappa_1 E^{BEMC}_{cl1}}{\mathcal{R}_1 \sqrt{E^i_{cl1}(\theta)}} \right)^2 + \left(\frac{E^i_{cl2}(\theta) - \kappa_2 E^{LAr}_{cl2}}{\mathcal{R}_2 \sqrt{E^i_{cl2}(\theta)}} \right)^2 \tag{9}$$

where $\mathcal{R}_1 = 0.3$ is a resolution factor for the BEMC and $\mathcal{R}_2 = 0.6$ for the LAr [8] (for more details on this method see [3]), κ_1 and κ_2 are the calibration factors for the BEMC and the LAr respectively, deduced from the minimization of χ^2. In fact, this method is in between the two preceding ones.

Using the Gaussian fit values as reference, as before, the following ratios are obtained:

- Data: $\kappa_2/\kappa_G = 0.924 \pm 0.015$
- Monte Carlo: $\kappa_2/\kappa_G = 0.989 \pm 0.007$

The figures (11-b,d) show the dependence of the ratio κ_2/κ_G on the energy and the dependence of the LAr wheels obtained by minimizing the χ^2. One sees that the calibration factors are lower than those obtained by the mean value (the ratio is lower), for both data and Monte Carlo. One observes a compatibility between this method and the mean value method for the behaviour of the dependence. Nevertheless, the discrepancy between data and Monte Carlo for the first energy bin, which appears especially in the CB2 area, is still there (figure 11-d).

5 The calibration factors - combined results

5.1 The combined results of the QED Compton and DIS NC (1+1) jet sample

In the previous section the results of the LAr calibration were considered independently for both the NC DIS (1+1) jet and the QED Compton sample. In the following the samples are treated together. The weighted average of the two samples leads to a calibration factor of 1.035 ± 0.005 for the entire LAr calorimeter. The error includes the systematic effects. In case of the jet

[8] One verifies, a posteriori, that these errors are realistic, because in this case the χ^2 per degree of freedom must be close to 1.

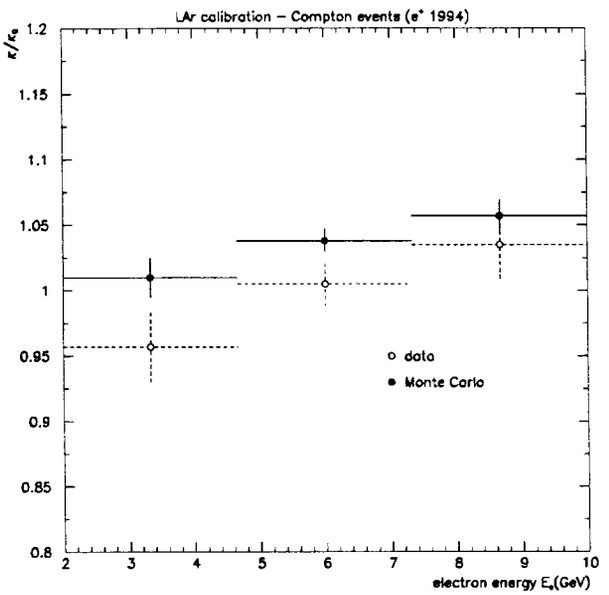

(a) The ratio of the calibration factors κ/κ_G by energy bins.

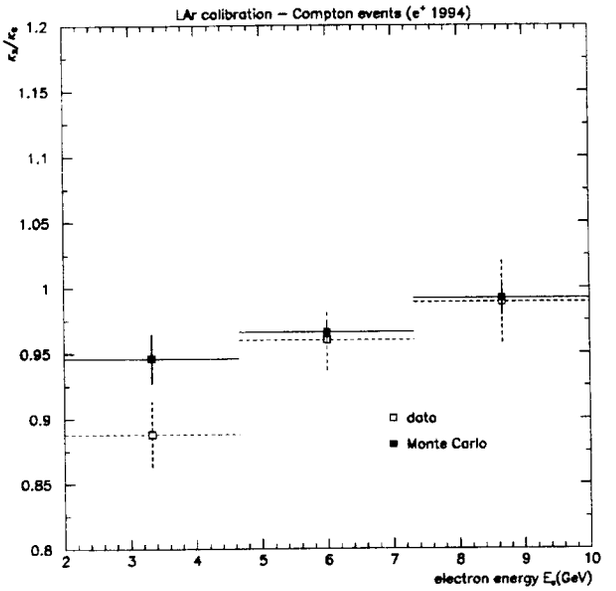

(b) The ratio of the calibration factors κ_2/κ_G by energy bins.

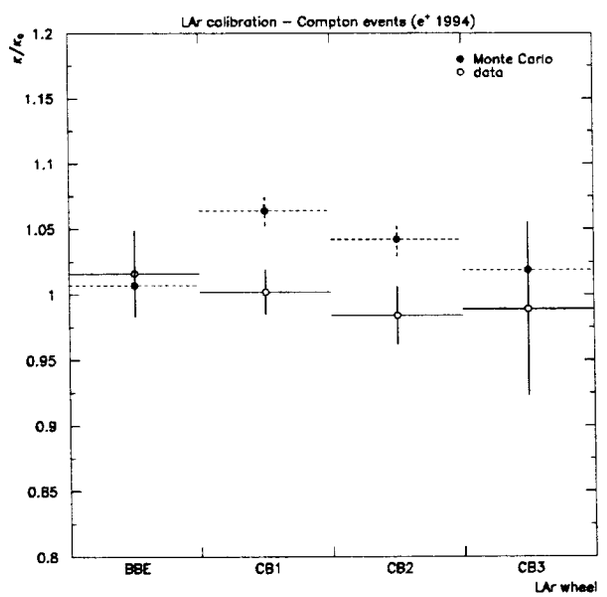

(c) The ratio of the calibration factors κ/κ_G by LAr wheel.

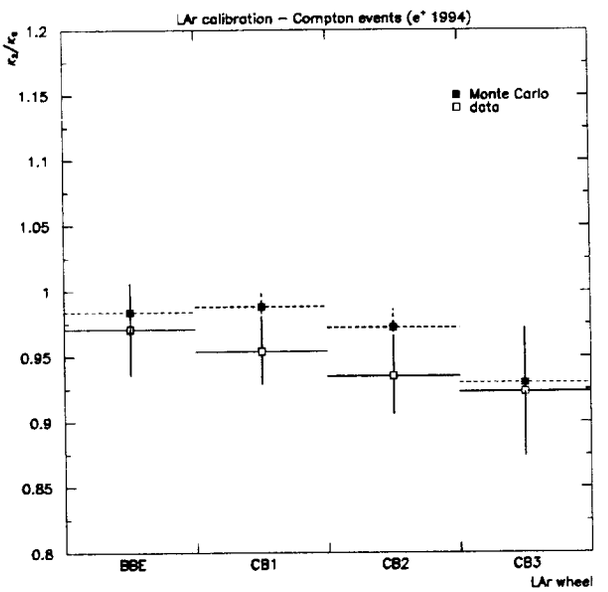

(d) The ratio of the calibration factors κ_2/κ_G by LAr wheel.

Figure 11: The deviation of the calibration factor (κ_G), when using the mean value (κ) and the χ^2 (κ_2) method .

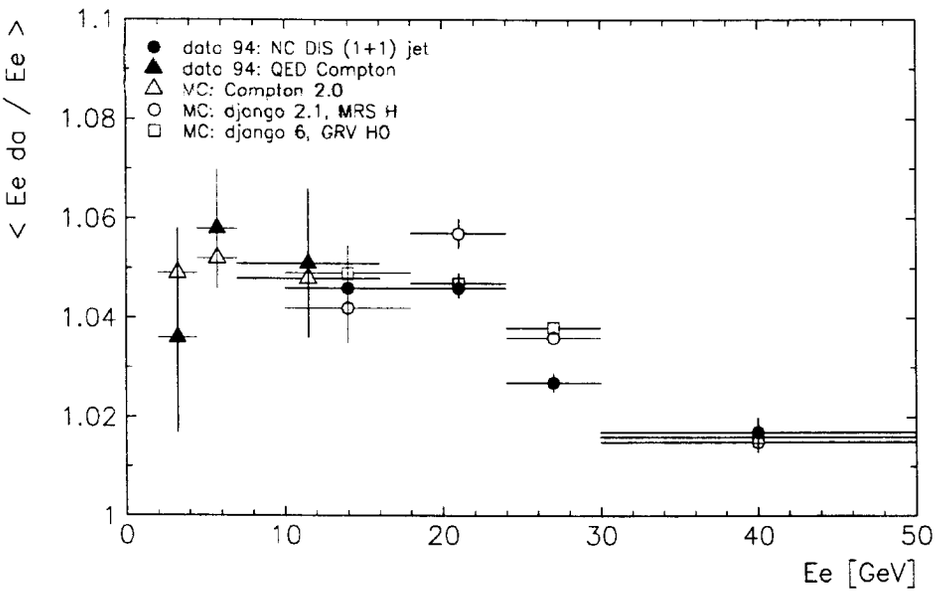

(a) The calibration factor E_e^{da}/E_e.

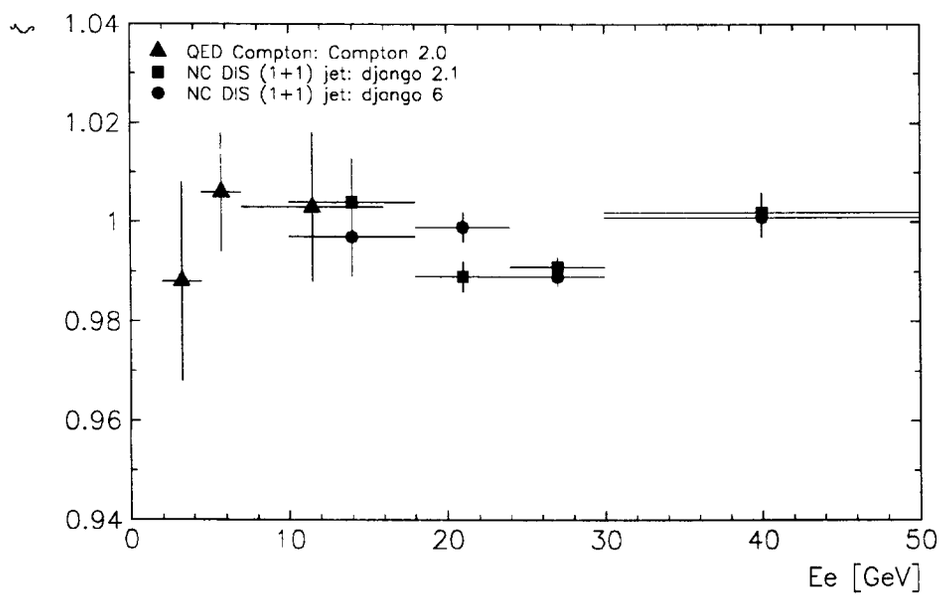

(b) The deviation of data and Monte Carlo ζ.

Figure 12: The calibration factor and the deviation of data and Monte Carlo as function of the double angle positron energy prediction for both the NC DIS (1+1) jet and QED Compton sample.

sample the difference of the peak positions of the fit to the increasing part of the distribution and the one to the decreasing part is used as systematic error (see section 4.1.3), while for the QED Compton sample the difference of the peak position of the Gaussian fit and the mean value is considered (see section 4.2.3). The calibration factors of the different calorimeter wheels are summarized in table 8.

Combining the samples, the predicted positron energy covers an energy range of 2 GeV to 50 GeV. The energy dependence of the calibration factors is shown in figure 12-a. At low energies, the calibration factor is about 1.04 and decreases to 1.02 at the highest energy values. The quality of the description of the measurement by Monte Carlo simulations is illustrated in figure 12-b, where the energy dependence of the ratio of the calibration factors of data to Monte Carlo is shown. The deviations over the entire energy range are everywhere less than 1 %.

LAr calor.	QED Compton	NC DIS (1+1) jet	combined samples
BBE	$1.071 \pm 0.024 \pm 0.016$	$1.021 \pm 0.003 \pm 0.008$	1.024 ± 0.008
CB1	$1.065 \pm 0.011 \pm 0.002$	$1.035 \pm 0.002 \pm 0.005$	1.040 ± 0.005
CB2	$1.035 \pm 0.015 \pm 0.016$	$1.025 \pm 0.003 \pm 0.004$	1.025 ± 0.005
CB3	$0.997 \pm 0.050 \pm 0.016$	$1.036 \pm 0.010 \pm 0.004$	1.034 ± 0.011
all	$1.048 \pm 0.008 \pm 0.001$	$1.028 \pm 0.001 \pm 0.006$	1.035 ± 0.005

Table 8: The calibration factors of the LAR calorimeter obtained from a weighted average of both the calibration factors of the NC DIS (1+1) jet and the QED Compton sample. The first part of the error is statistical, the second one is systematic.

5.2 The effect of an increased dead material correction

A study of E/p for low energy electrons from cosmic μ events has shown that Monte Carlo simulations do not describe the data. An increase of the dead material correction in the first layer of the LAr calorimeter by a factor 1.45 in case of data leads to a good agreement of data and Monte Carlo.

In order to specify the effect of the increased dead material correction the ratio of the calibration factor with the old dead material correction to the one with the new dead material correction

$$\rho = \frac{(\frac{E_e^{da}}{E_e})_{old}^{dead}}{(\frac{E_e^{da}}{E_e})_{new}^{dead}} \tag{10}$$

is defined.

The new dead material correction increases the observed positron response. Averaged over the entire LAr calorimeter in case of the NC DIS (1+1) jet sample $\rho = 1.007 \pm 0.001$ is found. The width obtained from a Gaussian fit to the increasing part of the distribution E_e^{da}/E_e does not change. In case of the QED Compton sample as average over the entire LAr calorimeter $\rho = 1.020 \pm 0.011$ is measured. Changes of the width are not observed. Within the errors for both samples no systematic dependence of ρ on the LAr calorimeter area is observed.

A small energy dependence of ρ is observed and illustrated in figure 13-a for both the NC DIS (1+1) jet and the QED Compton sample. At low energies, ρ is about 1.02 and decreases at high energies to 1.006.

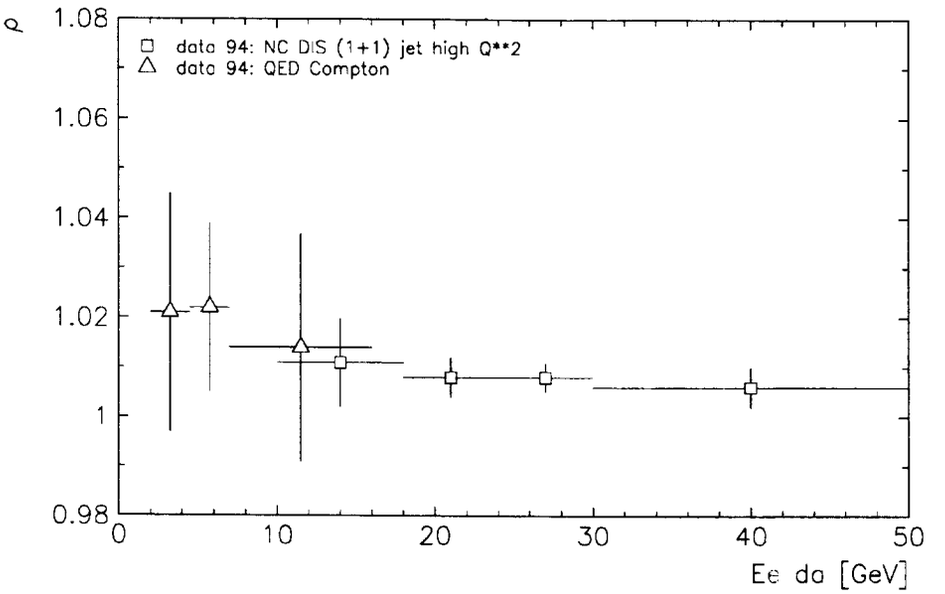

(a) The dependence of the ratio of the calibration factor with the old dead material correction to the calibration factor with new dead material correction on the predicted positron energy.

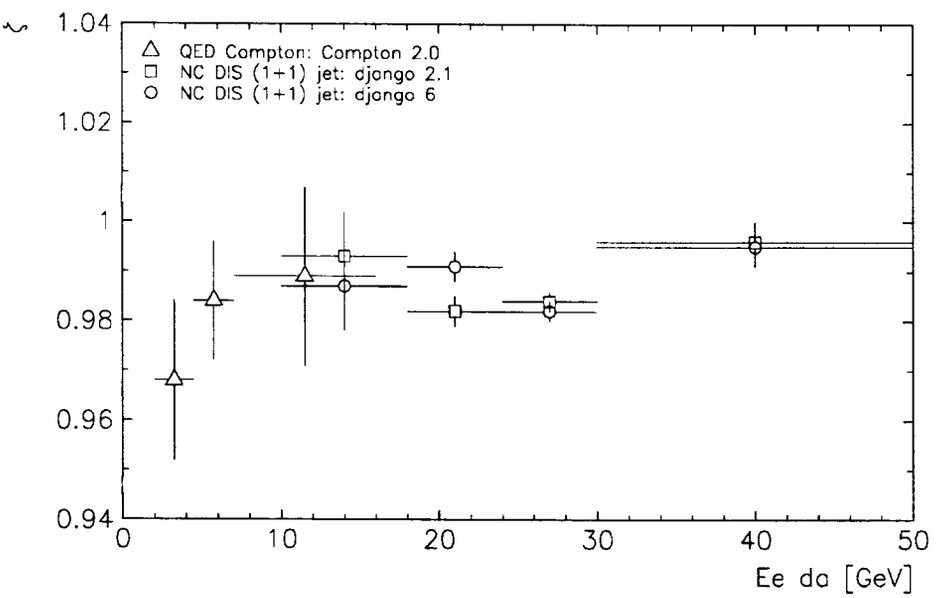

(b) The ratio of the calibration factor for data to the calibration factor for Monte Carlo as function of the predicted energy.

Figure 13: The dependence of ρ and ζ on the predicted positron energy for both the NC DIS (1+1) jet and the QED Compton sample.

Since the response to positrons due to the dead material correction increased, the ratio ζ decreased. This leads in case of the NC DIS (1+1) jet sample in the BBE to a deviation of data from MC to almost 4 %. In the CB area within the errors ζ is found to be about one. For the QED Compton sample in BBE $\zeta = 0.956 \pm 0.027$ is evaluated, while in the CB area ζ is clearly below one. In figure 13-b the energy dependence of ζ on the predicted positron energy for both the NC DIS (1+1) jet and the QED Compton sample is shown.

In summary, it can be concluded that the new dead material correction changes the energy scale on the 1% level with an increase at low energies, and the ratio data over Monte Carlo is clearly shifted below one.

6 The calibration of the central tracking system

The same method which has been applied to calibrate the LAr calorimeter can serve also for the calibration of the central tracking detector (CT). The energy spectrum of the positrons of the QED Compton events is just in the energy domain where the resolution of the tracking detectors is still good. In case of the NC DIS (1+1) jet events the transverse momentum of the positron needs to be restricted to values below 20 GeV.

In addition to the event selection explained in section 2.1 further restrictions have to be applied to the (1+1) jet sample:

- the track belonging to the positron has to be isolated ($\delta\eta > 1.0$ and $\delta\varphi > \pi/4$, where δ is the distance to the next track) $\Rightarrow$ to remove events where the positron produced an electromagnetic shower before or within central tracking detector.
- the number of the hits measured in the central jet chamber has to be bigger than 40 $\Rightarrow$ to be sure that the track is well measured.

In case of the QED Compton sample no additional selection criteria were applied.

The transverse momentum predicted by the double angle methods p_t^{da} is obtained by

$$p_t^{da} = E_e^{da} \sin\theta_e \tag{11}$$

where θ_e is the positron angle measured with the tracking system and E_e^{da} is the predicted positron energy by the double angle methods (QED Compton and NC).

The figure 14 shows the distributions of the ratio of the measured transverse momentum using the central tracking detector p_t^{trk} and the predicted transverse momentum p_t^{da} for both the QED Compton (figure 14-a,b) and the NC DIS (1+1) jet (figure 14-c) sample. The peak position of the distributions obtained by a symmetrical Gaussian fit represent the calibration factors of the central tracking system. The results are summarized in table 9. The QED Compton sample provides a calibration factor at low p_t^{da} ($< p_t^{da} > = 4.3$ GeV) which shows a deviation of 2.7 ± 0.8 %. In case of the NC DIS (1+1) jet events the deviation is measured to be 11.9 ± 0.6 % ($< p_t^{da} > = 14.2$ GeV).

The comparison to the Monte Carlo simulations in figure 14 and table 9 demonstrates that the experimental results are not at all described by the Monte Carlo, especially the resolution of p_t^{trk}/p_t^{da} which is about a factor 2 bigger in case of data.

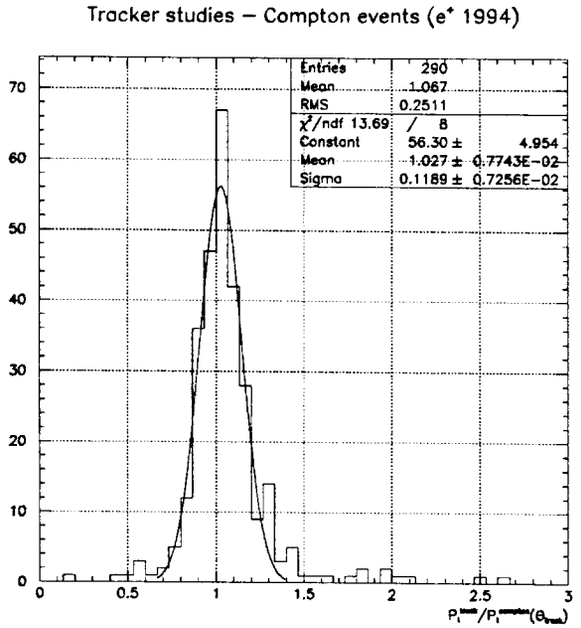

(a) The ratio p_t^{trk}/p_t^{da} for data.

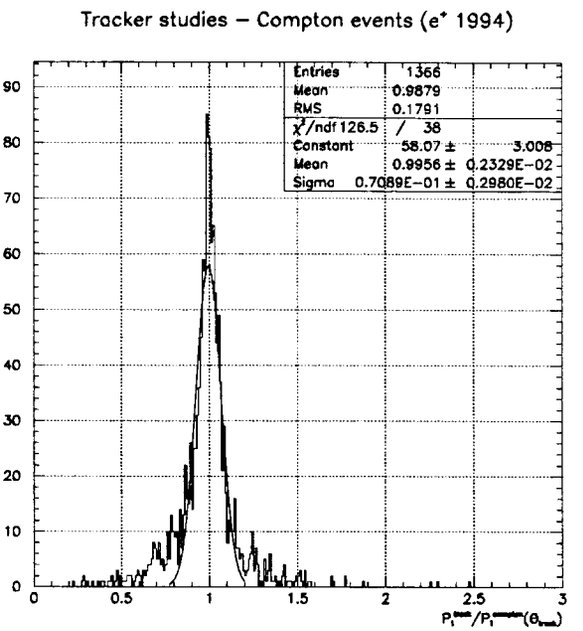

(b) The ratio p_t^{trk}/p_t^{da} for Monte Carlo.

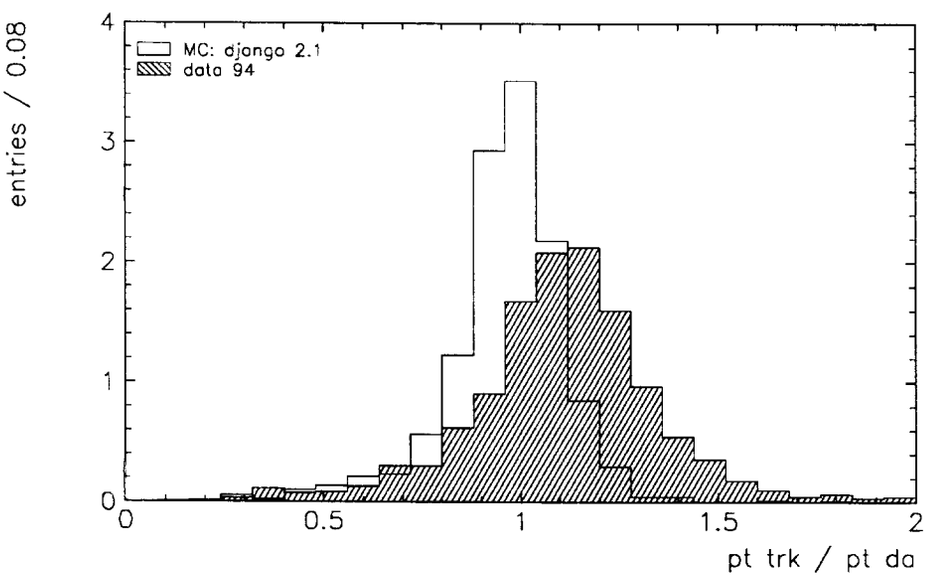

(c) The ratio of p_t measured with the central tracking system to the predicted p_t by double angle in case of NC DIS (1+1) jet events for data and MC.

Figure 14: The ratio p_t^{trk}/p_t^{da} in case of QED Compton and NC DIS (1+1) jet events for data and Monte Carlo.

	data 94	Monte Carlo
NC DIS (1+1) jet		
p_t^{trk}/p_t^{da}	1.118 ± 0.006	0.981 ± 0.003
σ	0.200	0.116
N_{event}	1326	1567
QED Compton		
$p_t^{trk}/p_t^{compton}$	1.027 ± 0.008	0.996 ± 0.002
σ	0.119	0.071
N_{event}	290	1366

Table 9: The summary of the calibration factors of the central tracking system in case of QED Compton and NC DIS (1+1) jet events for data and Monte Carlo.

The previous results suggest a p_t dependence of the calibration factors of the central tracking system. In the following, both samples are merged and treated together. The peak position of the distributions of p_t^{trk}/p_t^{da} are determined by Gaussian fits in bins of p_t^{da}. The values obtained for both data and MC are shown in figure 15. In case of data (full symbols) the calibration factors increase linearly with p_t and a linear fit yields

$$\frac{p_t^{trk}}{p_t^{da}} = (0.0091 \pm 0.001)p_t^{da} + (0.99 \pm 0.01) \tag{12}$$

Clearly, the Monte Carlo simulation (open symbols) does not reproduce this behaviour.

In order to summarize: a p_t dependent calibration factor for the central tracking system[9] (0.9 % per GeV in p_t) seems to be necessary in case of data. The experimental results are not reproduced by the Monte Carlo simulation. The question is, how this extrapolates to the region of p_t of about 1 GeV, where a deviation of 1 % would be expected from these studies.

7 Conclusion

Combining the results of both, the NC DIS (1+1) jet and QED Compton sample, a calibration factor averaged over the CB and BBE part of the LAr calorimeter was measured to be 1.035 ± 0.005. The Monte Carlo simulations show an agreement better than 1 % with respect to the data. The calibration of the central tracking detector results in a linear dependence of the calibration factor on the true transverse momentum ($p_t^{trk}/p_t^{da} = (0.0091 \pm 0.001)p_t^{da} + (0.99 \pm 0.01)$).

[9]Further studies by C. Niebuhr et al. relate the slope to a rotation of the central tracking detector. This problem will be solved on the calibration level for the reprocessing of the data taken during 1995.

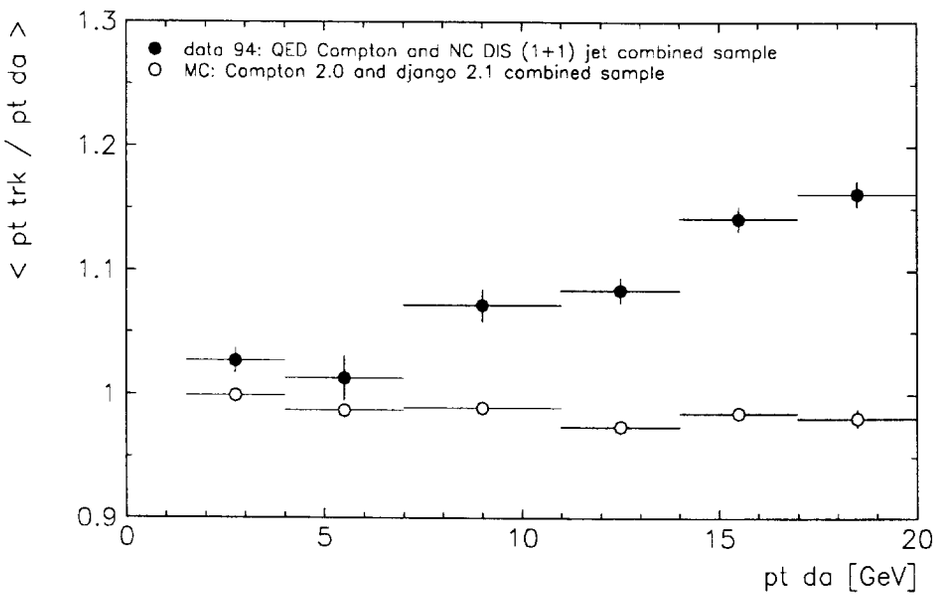

Figure 15: The ratio $< p_t^{trk}/p_t^{da} >$ obtained by symmetrical Gaussian fit in various bins of p_t^{da} in case of a merged sample of QED Compton and NC DIS (1+1) jet events for data and Monte Carlo simulation.

Appendix

Starting from the definition of QED Compton events and their characteristics explained above the following cuts were applied to select them :

We remind that only LAr and BEMC clusters are taken into account; they are ordered by decreasing energy for each detector:

$$E_{cl1}^{lar} \geq E_{cl2}^{lar} \geq E_{cl3}^{lar} \geq .....$$
$$E_{cl1}^{bemc} \geq E_{cl2}^{bemc} \geq E_{cl3}^{bemc} \geq .....$$

A)- Global cuts :

- Cut on the vertex : $-100 \leq z_{vrtx} \leq 150cm$ or no reconstructed vertex.
- Cut on the number of tracks : Number of good tracks (DTRA) ≤ 3 .

Since in 1993 we had the problem of the loss of events by the cut on the energy of the third cluster at 2 GeV. A noisy cluster in the LAr with an energy higher than 2 GeV added to the two real clusters of the Compton event, contribute to the rejection of this one, if we ask not more than two clusters in the calorimeters. And since we can not relax completely the cut on the third clusters energy, we decided to add some constraints to our cuts. So, our selection is an "OR" of two subselections. The first one is dedicated to the calibration of the calorimeters,

so it has to be completely free from any energy constraints and does not suffer from the loss of events. In this case we use the '93 selection with a cut on the third cluster's energy at 2 GeV. The second subselection is done such a way that we do not loose any event. This is clear if we want to measure the luminosity with such events. In the following we detail these two subselections [10].

B)- Calibration-oriented cuts :

- BEMC/BEMC events :
  - * Cut on the visible energy : $E_{cl1}^{bemc} + E_{cl2}^{bemc} \geq 18$ GeV
  - * $E_{cl1}^{bemc} \geq 8$ GeV
  - * $E_{cl2}^{bemc} \geq 4$ GeV
  - * Cut on the third cluster's energy $E_{cl3}^{bemc} < 2$ GeV & $E_{cl1}^{lar} < 2$ GeV
  - * Cut on the coplanarity angle : $\frac{3\pi}{4} \leq \Delta\varphi \leq \frac{5\pi}{4}$ ($|\pi - \Delta\varphi| \leq 45^o$).
  - * $E_{cl1}^{bemc} + E_{cl2}^{bemc} \leq 32$ GeV

- For BEMC/LAr and LAr/LAr events:

BEMC/LAr events :

  - * $E_{cl1}^{bemc} + E_{cl1}^{lar} \geq 18$ GeV
  - * $E_{cl1}^{bemc} \geq 8$ GeV
  - * $E_{cl1}^{lar} \geq 2$ GeV
  - * Cut on the third cluster's energy $E_{cl2}^{bemc} < 2$ GeV & $E_{cl2}^{lar} < 2$ GeV
  - * Cut on the coplanarity angle : $\frac{3\pi}{4} \leq \Delta\varphi \leq \frac{5\pi}{4}$ ($|\pi - \Delta\varphi| \leq 45^o$).

LAr/LAr events :

  - * $E_{cl1}^{lar} + E_{cl2}^{lar} \geq 18$ GeV
  - * $E_{cl1}^{lar} \geq 8$ GeV
  - * $E_{cl2}^{lar} \geq 2$ GeV
  - * Cut on the third cluster's energy $E_{cl1}^{bemc} < 2$ GeV & $E_{cl3}^{lar} < 2$
  - * Cut on the coplanarity angle : $\frac{3\pi}{4} \leq \Delta\varphi \leq \frac{5\pi}{4}$ ($|\pi - \Delta\varphi| \leq 45^o$).

C)- Luminosity-oriented cuts :

In this case we accept a maximum of 4 clusters in LAr and BEMC having more than 2 GeV ($E_{cl5} < 2$ GeV for BEMC and LAr), and try to find 2 (BEMC or LAr) clusters combination and accept the event if:

- they pass the same cuts as above, without the cut on the third BEMC or LAr cluster energy.

&

[10] Note that we use the BCFR scale for the BEMC and ACLR scale for the LAr. One calls BEMC/BEMC, BEMC/LAr and LAr/LAr events those having the two final particles in the BEMC, one particle in the BEMC and the other in the LAr and both the particles in the LAr respectively.

– Cut on the BEMC cluster's radius $R_{cl}^{bemc} \leq 6cm$.

&

– The combination of the 2 clusters must have (remember that for '93 data, one has chosen a cut of $\chi^2 \leq 12$ for the luminosity measurement) :

$$\chi^2 = \sum_{i=1}^{2} \left(\frac{E_{cl}^i(\theta) - E_{cl}^i}{0.3\sqrt{E_{cl}^i(\theta)}} \right)^2 \leq 25$$

So the event is classified QED Compton if (A).and.[B).or.C)]) is right.

References

[1] A.Courau and P.Kessler, Physical review D33(1986) 2024-2028

[2] A.Courau and P.Kessler, Physical review D46 1(1992) 117-124

[3] S. Kermiche, PhD thesis, LAL 94-14, 1994.

[4] A. Pieuchot, J. Marks, C. Vallée, Pile up energy detection using the LAr Big Tower Timing information, H1-01/95-423

[5] H1note : A.Courau, H1-07/91-187

[6] A.Courau et al., Proc. Workshop on Physics at HERA, DESY, Hamburg(1991), vol. 2, p. 902

[7] T.Carli et al., Proc. Workshop on Physics at HERA, DESY, Hamburg(1991), vo. 3, p. 1468

[8] S. Bentvelsen et al., Proceedings of the HERA-92 workshop, vol. 1

[9] C. Hoeger, Proceedings of the HERA-92 workshop, vol. 1

[10] H1note : A. Courau and S.Kermiche H1-12/92-260

[11] H1note : A. Courau and S.Kermiche H1-10/93-321

[12] H1 collaboration, T. Ahmed et al., Z. Phys. C66(1995)529.

List of Figures

1 The processes considered for the calibration of the electromagnetic scale of the LAr calorimeter, a) NC DIS (1+1) jet process, b) QED Compton process. 4

2 The Q^2 and y distributions of data and both Monte Carlo sets for NC DIS (1+1) jet events after selection. 6

3 The Compton estimators distributions (a) and (b) and a schematic view of the cluster positions for the final data sample (c). 9

4 The data and Monte Carlo comparisons for the final sample: the energy E_e, the angles θ_e and φ_e of the positron in the LAr. 10

5 The ratio of the double angle energy prediction to the positron energy (E_e^{da}/E_e), (a) at the generator level, (b) after reconstruction and selection, for the data and the two Monte Carlo samples. 12

6 The ratio of the predicted Compton energy to the energy at the generator level ($E_e(\theta)/E_e^{gen}$) (a) and its energy dependence (b). 13

7 The calibration factor E_e^{da}/E_e as function of the positron double angle energy : (a) For data and the two Monte Carlo samples after reconstruction and selection, (b) at the generator level. 15

8 The dependence of the calibration factor on the energy of the positron and on the jet angle. Monte Carlo and data comparison. 16

9 The distributions of calibration factor ($E_e(\theta)/E_e$) for data and Monte Carlo. . . 21

10 The dependence of the calibration factor and the data to Monte Carlo ratio, with the energy and the LAr wheels. 22

11 The deviation of the calibration factor (κ_G), when using the mean value (κ) and the χ^2 (κ_2) method 24

12 The calibration factor and the deviation of data and Monte Carlo as function of the double angle positron energy prediction for both the NC DIS (1+1) jet and QED Compton sample. 25

13 The dependence of ρ and ζ on the predicted positron energy for both the NC DIS (1+1) jet and the QED Compton sample. 27

14 The ratio p_t^{trk}/p_t^{da} in case of QED Compton and NC DIS (1+1) jet events for data and Monte Carlo. 29

15 The ratio $< p_t^{trk}/p_t^{da} >$ obtained by symmetrical Gaussian fit in various bins of p_t^{da} in case of a merged sample of QED Compton and NC DIS (1+1) jet events for data and Monte Carlo simulation. 31

List of Tables

1 The parameter summary of the generated NC Monte Carlo event samples. 5

2 The number of NC DIS (1+1) jet events after the selection. 7

3 The calibration factors in various parts of the LAr calorimeter. 17

4 The ratio of data to Monte Carlo in various parts of the LAr calorimeter. 18

5 The calibration factors of BBE and CB1 for different octants. 18

6 The calibration factors and the ratio of data to Monte Carlo in various energy bins. 19

7 The calibration factors and data to Monte Carlo ratio by LAr wheels. 20

8 The calibration factors of the LAR calorimeter obtained from a weighted average of both the calibration factors of the NC DIS (1+1) jet and the QED Compton sample. The first part of the error is statistical, the second one is systematic. . . 26

9 The summary of the calibration factors of the central tracking system in case of QED Compton and NC DIS (1+1) jet events for data and Monte Carlo. 30